

1 **Impact of intraseasonal wind bursts on SST variability in the**
2 **far eastern Tropical Atlantic Ocean during boreal spring**
3 **2005 and 2006. Focus on the mid-May 2005 event.**

4 Gaëlle Herbert¹, Bernard Boulès¹

5 ¹:Institut de Recherche pour le Développement (IRD), Laboratoire d'Etudes Géophysiques et Océanographie Spatiale
6 (LEGOS), Brest, France.

7 *Correspondence to:* Gaëlle Herbert (gaelle.herbert@ird.fr)

8

9 **Abstract.** The impact of boreal spring intraseasonal wind bursts on sea surface temperature variability in the
10 eastern Tropical Atlantic Ocean in 2005 and 2006 is investigated using numerical simulation and observations.
11 We specially focus on the coastal region east of 5° E and between the equator and 7° S that has not been studied
12 in detail so far. For both years, the southerly winds strengthening induced cooling episodes through i) upwelling
13 processes; ii) vertical mixing due to vertical shear of the current; and for some particular events iii) a decrease
14 of incoming surface shortwave radiation. The strength of the cooling episodes was modulated by subsurface
15 conditions affected by the arrival of Kelvin waves from the west influencing the depth of the thermocline. Once
16 impinging the eastern boundary, the Kelvin waves excited westward-propagating Rossby waves which,
17 combined with the effect of enhanced westward surface currents, contributed to the westward extension of the
18 cold water. A particularly strong wind event occurred in mid-May 2005 and caused an anomalous strong cooling
19 off Cape-Lopez and in the whole eastern Tropical Atlantic Ocean. From the analysis of oceanic and atmospheric
20 conditions during this particular event, it appears that anomalous strong boreal spring wind strengthening
21 associated to anomalous strong Hadley cell activity made the event as a decisive event which prematurely
22 triggered the rainfall coastal onset in the northern Gulf of Guinea, making it the earliest over 1998-2008 period.
23 Results show that no similar atmospheric conditions were observed in May over the 1998-2008 period. It is also
24 found that the anomalous oceanic and atmospheric conditions associated to the event exerted strong influence on
25 rainfall off Northeast Brazil. This study highlights the different processes through which the wind power from
26 South Atlantic is brought to the ocean in the Gulf of Guinea and emphasizes the need to further document and
27 monitor the South Atlantic region.

28

29 **1.Introduction**

30 The eastern equatorial Atlantic Ocean shows a pronounced seasonal cycle in sea surface temperature (SST)
31 (Wauthy, 1983; Mitchell and Wallace, 1992). One strong signature of the SST seasonal cycle in the eastern
32 equatorial Atlantic is the Atlantic cold tongue (ACT) (Zebiak, 1993) characterized by a fast drop of SST (up to
33 7° C) in boreal spring and summer slightly south of the equator and east of 20°W (Merle, 1980; Picaut, 1983).

34 During boreal summer, the southern boundary of this cooler temperature connects progressively with the austral
35 winter cooling of the Southern hemisphere SSTs. A number of observational (Merle, 1980; Foltz et al., 2003)
36 and modeling (Philander and Pacanowski, 1986; Yu et al., 2006; Peter et al., 2006) studies show that the
37 development of the ACT is driven by the seasonal increase of the Southern Hemisphere trade winds during late
38 boreal winter to early summer (Brandt et al., 2011) associated to the meridional displacement of the Inter-
39 Tropical Convergence Zone (ITCZ) (Picaut, 1983; Colin, 1989; Waliser and Gautier, 1993; Nobre and Shukla,
40 1996). The equatorial cooling would be regulated by a coupling between thermocline shoaling, subsurface
41 dynamics (Yu et al., 2006; Peter et al., 2006; Wade et al., 2011; Jouanno et al., 2011) including turbulent
42 mixing, vertical advection and entrainment, as well as horizontal advection. The equatorial thermocline shoaling
43 is the consequence of local and remote wind forcing: the strengthening of easterly winds in the western
44 equatorial Atlantic remotely forces the seasonal upwelling in the eastern part of the basin via equatorial Kelvin
45 waves (Moore et al., 1978; Adamec and O'Brien, 1978; Busalacchi and Picaut, 1983; McCreary et al., 1984).

46 Besides the dominant seasonal cycle, the eastern tropical Atlantic is under the influence of meridional southerly
47 winds (Picaut, 1984) which fluctuate with a period close to 15 days (Krishnamurti, 1980; de Coëtlogon et al.,
48 2010; Jouanno et al., 2013). These intraseasonal wind fluctuations are therefore expected to be a major
49 contributor to the seasonal SST cooling and their fluctuations occur as a vector of energy and momentum from
50 the South Atlantic to the eastern equatorial Atlantic. A connection between the strength of the St. Helena
51 Anticyclone and SST anomalies in the southeastern tropical Atlantic has been described by Lübbecke et al.
52 (2014). These authors suggest that the St. Helena Anticyclone variability might be an importance source of
53 anomalous tropical Atlantic wind power which affects SST in the eastern equatorial Atlantic via several
54 mechanisms: zonal wind stress changes in the western equatorial basin, wave adjustment, meridional advection
55 of subsurface temperature anomalies, intraseasonal wind stress variations, and possibly even other mechanisms.
56 Through the in situ data analysis of AMMA/EGEE cruises (Redelsperger et al., 2006; Bourlès et al., 2007)
57 carried out in 2005 and 2006, Marin et al. (2009) show that the SST seasonal cooling at the equator east of 10°
58 W is not smooth but results from the succession of short-duration cooling episodes generated by southeasterly
59 wind bursts due to the fluctuating St. Helena Anticyclone. In addition, according to Leduc-Leballeur et al.
60 (2013), the sharp and durable change in the atmospheric circulation in the northern Gulf of Guinea (durably
61 strong southerlies north of equator) takes place through an abrupt seasonal transition prepared by a succession of
62 southerly wind bursts and possibly triggered by a significantly stronger wind burst. The southerly wind bursts
63 occurring in boreal spring in the Gulf of Guinea thus would play an important role in driving precipitation
64 pattern in the area through air-sea interactions (de Coëtlogon et al., 2010; Nicholson and Dezfuli, 2013) and
65 coupling between the ACT and the West Africa Monsoon (WAM).

66 Improving our understanding of the impact of such wind bursts on SST variability at intraseasonal scale in the
67 eastern Tropical Atlantic is important through its link with the regional climate. However, while the ACT and
68 Angola-Benguela regions have been the object of many studies, the dynamics and SST variability of the coastal
69 eastern region is much less documented.

70 In this study, we therefore first focus our analysis off Cape-Lopez (defined from 0° N-7° S; 5° E-14° E and
71 hereafter called CLR for ‘Cape-Lopez region’) and aim to improve understanding of its seasonal SST variability
72 and the impact of intraseasonal winds on SST variability during boreal spring and summer. To this end, we use
73 regional high resolution model results as well as satellite SST data and sea surface height observations. We first
74 use model outputs from 1998 to 2008 to analyze the seasonal cycle in CLR and to highlight its interannual
75 variability, and then we specially focus on the years 2005 and 2006 to investigate the SST response of
76 intraseasonal wind forcing. These two particular years were largely investigated during the African Monsoon
77 Multidisciplinary Analyses (AMMA) experiment (Redelsperger et al., 2006). The year 2005 is characterized by
78 the lowest SST values in the ACT during the past 3 decades (along with 1982), while 2006 is considered as a
79 normal year (Caniaux et al., 2011). Also, 2005 exhibits the earliest development of the ACT. The study of SST
80 variability at intraseasonal scale during these two years is thus interesting for better understanding their
81 observed differences in SST seasonal conditions. These two particular years have been also chosen by Marin et
82 al. (2009) to study the variability of the properties of the ACT. Their study concerned the equatorial area west of
83 4° E, whereas we propose to focus in CLR, east of 5° E where coastal processes are expected to be involved.

84 The question of the processes implied in the SST variability in the Cape-Lopez region was raised based on an
85 observation in satellite SST data of cold coastal waters during boreal spring independent from those observed
86 off shore in the cold tongue region around 10°W which also raised the question of the link of such cooling with
87 the cold tongue development. Most studies on the CLR focused on the analysis of observational dataset to
88 examine the hydrology and its seasonal variation along the frontal (coastal) region of Congo (e.g. Merle, 1972;
89 Piton, 1988) or on the impact of Congo River on SST and mixed layer (e.g. Matera et al., 2012; Denamiel et al.,
90 2013; White and Toumi, 2014) but, to our knowledge, no detailed analysis of SST variability at seasonal and
91 intraseasonal time scales have been realized. A better understanding of ocean-atmosphere interactions in this
92 region is thus needed. Some previous studies related to the whole eastern Tropical Atlantic (Gulf of Guinea)
93 suggest that multiple processes could be in play in the CLR, coupling remote and local forcing, and combined
94 with the very low thermal inertia of the mixed layer depth. For example, Giordani et al. (2013) show from
95 regional model results that horizontal advection, entrainment, and turbulent mixing significantly contribute to
96 the heat budget east of 3°W because of the very thin mixed layer. The upper layers of the north CLR might also
97 be impacted by vertical mixing induced by the intense current vertical shear between the South Equatorial
98 Current, flowing westward at the surface, and the subsurface eastward Equatorial Under-Current. In addition to
99 local forcing, the area is also under the influence of the arrival of equatorial Kelvin waves from West and their
100 reflection, once reaching the African coast, poleward as coastally trapped waves and westward as Rossby waves
101 (Moore, 1968; McCreary, 1976; Moore and Philander, 1977). The principal source of the equatorial Kelvin
102 waves has been usually related to the western equatorial zonal wind changes during late boreal winter to early
103 summer (e.g.; Philander, 1990). In order to better understand the trigger mechanism of Kelvin waves generation
104 which conditions the mixed layer properties in the CLR, another purpose of this study is thus to identify the
105 atmospheric conditions coinciding with the Kelvin waves generation in the West of the basin during winter 2005
106 and 2006. In addition, some studies (such as DeCoëtlogon et al., 2010) suggest that at short time scale (a few

107 days), more than half of the cold SST anomaly around the equatorial cooling could be explained by horizontal
108 oceanic advection of upwelled cold coastal waters controlled by the winds. Therefore, a better understanding of
109 the SST variability in the CLR may also help to better understand the SST variability in the equatorial region.

110 Several studies (*e.g.* Okumura and Xie, 2004; Caniaux et al., 2011; Nguyen et al., 2011; Thorncroft et al., 2011)
111 show evidence of a high correlation between the ACT and the WAM onset in the Sahelian region. Based on an
112 analysis of 27 years of data, Caniaux et al. (2011) identified the year 2005 as the year with the earliest WAM
113 onset date (around 19 May 2005 whereas they define the mean onset date on 23 June \pm 8 days). According to
114 Marin et al. (2009), the time shift in the development of the ACT between 2005 and 2006 is related to a
115 particular wind burst event in mid-May 2005. This mid-May 2005 event therefore appears as exerting a strong
116 influence on the WAM. In a second part of the study, we thus focus on this particular wind event that preceded a
117 strong cold event in the far eastern Tropical Atlantic along with an early ACT development. We aim to describe
118 i) the atmospheric and oceanic conditions during this particular event; ii) to what extent it is involved in the
119 WAM system; and iii) which processes make it an exceptional event.

120 The remainder of the paper is organized as follows. In Sect. 2, the model and observational data used in this
121 study are described. The seasonal and interannual variability of SST, winds, currents, 20° C-isotherm depth and
122 sea surface heat flux in the CLR are analyzed in Sect. 3. The cooling episodes generated in response to southerly
123 wind bursts and the other forcing mechanisms implied in the CLR are investigated in details for the years 2005
124 and 2006 in Sect. 4. In Sect. 5, we focus our analysis on the unusual wind burst occurring in mid-May 2005.
125 Finally, the main results are summarized and discussed in Sect. 6.

126

127 **2. Model and data**

128 The numerical model used in this paper is the Regional Oceanic Modeling System (ROMS) (Shchepetkin and
129 McWilliams, 2005). The model configuration is the same as employed in Herbert et al. (2016), and the
130 following text is derived from there with minor modifications.

131 ROMS is a three-dimensional free surface, split-explicit ocean model which solves the Navier-Stokes primitive
132 equations following the Boussinesq and hydrostatic approximations. We used the ROMS version developed at
133 the Institut de Recherche pour le Développement (IRD) featuring a two-way nesting capability based on AGRIF
134 (Adaptative Grid Refinement In Fortran) (Debreu et al., 2012). The two-way capability allows interactions
135 between a large-scale (parent) configuration at lower resolution and a regional (child) configuration at high
136 resolution. The ROMSTOOLS package (Penven et al., 2008) is used for the design of the configuration. The
137 model configuration is built following the one performed by Djakouré et al. (2014) over the Tropical Atlantic.
138 The large scale domain extends from 60° W to 15.3° E and from 17° S to 8° N and the nested high resolution
139 zoom focuses between 17° S and 6.6° N and between 10° W and 14.1° E domain. This configuration allows for
140 equatorial Kelvin waves induced by trade wind variations in the western part of the basin to propagate into the
141 Gulf of Guinea and influence the coastal upwelling (Servain et al., 1982; Picaut, 1983). The horizontal grid

142 resolution is $1/5^\circ$ (i.e. 22 km) for the parent grid and $1/15^\circ$ (i.e. 7 km) for the child grid (see Herbert et al.
143 (2016), their Fig. 1). This allows an accurate resolution of the mesoscale dynamics since the first baroclinic
144 Rossby radius of deformation ranges from 150 to 230 km in the region (Chelton et al., 1998). The vertical
145 coordinate is discretized into 45 sigma levels with vertical S-coordinate surface and bottom stretching
146 parameters set respectively to $\theta_s = 6$ and $\theta_b = 0$, to keep a sufficient resolution near the surface
147 (Haidvogel and Beckmann, 1999). The vertical S-coordinate Hc parameter, which gives approximately the
148 transition depth between the horizontal surface levels and the bottom terrain following levels, is set to $H_c = 10$
149 m. The GEBCO1 (Global Earth Bathymetric Chart of the Oceans) is used for the topography (www.gebco.net).
150 The runoff forcing is provided from Dai and Trenberth's global monthly climatological run-off data set (Dai and
151 Trenberth, 2002). The rivers properties of salinity and temperature are prescribed as annual mean values. One
152 river (Amazon) is prescribed in the parent model while five rivers, that correspond to the major rivers present
153 around the Gulf of Guinea, are prescribed in the child model (Congo, Niger, Ogoou, Sanaga, Volta). At the
154 surface, the model is forced with the surface heat and freshwater fluxes as well as 6 hourly wind stress derived
155 from the Climate Forecast System Reanalysis (CFSR) (horizontal resolution of $1/4^\circ \times 1/4^\circ$) (Saha et al., 2010). Our
156 model has three open boundaries (North, South, and West) forced by temperature and salinity fields from the
157 Simple Ocean Data Analyses (SODA) (horizontal resolution of $1/2^\circ \times 1/2^\circ$) (Carton et al., 2000a, 2000b; Carton
158 and Giese, 2008). The simulation has been performed on IFREMER Caparnmor super-computer and integrated
159 for 30 years from 1979 to 2008 with the outputs averaged every 2 days. A statistical equilibrium is reached after
160 ~ 10 years of spin-up. Model analyses are based on the 2-days averaged model outputs from year 1998 to year
161 2008. The model has already been validated successfully with a large set of measurements and climatological
162 data, and more detailed information about the model validations can be found in Herbert et al. (2016).

163 Note that throughout the whole text and figure captions, the term “intraseasonal variations” is used to designate
164 the field obtained after the removing of the 30 days low-pass filtered field to the total field of the given year,
165 while “intraseasonal anomaly” refers to the field obtained after the removing of the 30 days low-pass filtered
166 field averaged over 1998-2008 to the total field of the given year.

167

168 For SST observations, we use data obtained from measurements made by the Tropical Rainfall Measuring
169 Mission microwave imager (TMI). The dataset is a merged product available at www.remss.com. The SST data
170 have a spatial resolution of $1/4^\circ$ and for the present study the 10 years' time series, from 1 January 1998 to 31
171 December 2008, obtained as 3-daily field. The important feature of the microwave retrievals is that it can give
172 accurate SST measurements under clouds (Wentz et al., 2000). However, the major limitation to the microwave
173 TMI observations is land contamination which results in biases of the order of 0.6°K within about 100 km from
174 the coast (Gentemann et al., 2010). Thus, in the Optimal Interpolation TMI product the offshore zone with no
175 data extends at approximately 100 km from the coast. This limits to some degree the analysis of near-coastal
176 regions, in particular those dominated by coastal upwelling dynamics.

177 We also use for this study daily sea surface height (SSH) data, which are available for the period 1993–2012 and
178 maintained by the organization for Archiving, Validation, and Interpretation of Satellite Oceanographic data

179 (AVISO; www.aviso.altimetry.fr). The sea surface height dataset is a merged product of observations from
180 several satellite missions Ssalto/Duacs (Segment Sol multimissions d'ALTimétrie, d'Orbitographie et de
181 localisation précise/Developing Use of Altimetry for Climate Studies) mapped onto a 0.25° Mercator projection
182 grid. All standard corrections have been made to account for atmospheric (wet troposphere, dry troposphere and
183 ionosphere delays) and oceanographic (electromagnetic bias, ocean, load, solid Earth and pole tides) effects.
184 The mean sea surface topography for the period 1993–2012 was removed from the SSH to produce sea surface
185 height anomalies.

186 In addition, surface pressure data were studied using ECMWF Atmospheric Reanalysis (ERA) for the 20th
187 Century product. The four-hourly data are daily averaged and is available on <https://rda.ucar.edu> website. The
188 product assimilates surface pressure and marine wind observations.

189

190 **3. Seasonal variability of surface conditions in CLR**

191 The purpose of this section is to describe the seasonal atmospheric and ocean surface conditions in the CLR.

192 The seasonal variability of SST, surface winds stress, horizontal current intensity, depth of 20° C-isotherm
193 (hereafter referred to as z20), and the surface net heat flux from monthly averaged model outputs in the CLR for
194 each year from 1998 to 2008 and averaged over the period are shown on Fig. 1. The reliability of the model is
195 also provided by comparing the simulated and the corresponding TMI SST climatological seasonal cycle in the
196 CLR (Fig. 1a). The SST variations display an annual cycle with highest temperature in boreal winter (warm
197 season), when the ITCZ reaches its southernmost position and the trade winds are weakest, and minimum values
198 in boreal summer (cold season), when the trades intensify. The most salient features of the atmospheric and
199 hydrographic fields during May-June are also illustrated on Fig. 1 by May-June averaged maps. Despite a warm
200 bias (~1°C) compared to satellite observations, the model well reproduces the satellite pattern. While this warm
201 bias in the eastern tropical Atlantic is well known in coupled climate models (e.g. Zeng et al., 1996; Davey et
202 al., 2002; Deser et al., 2006; Chang et al., 2007; Richter and Xie, 2008), results from Large and Danabasoglu
203 (2006) suggest indeed that a warm SST bias may also be present along the Atlantic coast of southern Africa in
204 forced ocean-only simulation. The SST May-June average map indicates that the boreal summer SST minimum
205 is related to intensified cool SST around 6°S, in the Congo mouth region. In this region, the coast is oriented
206 parallel to the trade flow which reinforces in boreal summer, thus favorable to coastal upwelling processes. The
207 mean alongshore wind stress during May-June reveals in fact that upwelling conditions are observed over most
208 of the CLR. Wind stress magnitude exhibits a semi-annual variability with a second maximum in October–
209 December and a weakening during July-September season (Fig. 1b). The strengthening of winds in boreal spring
210 is associated with a strengthening of mean current speed, particularly off Cape-Lopez between 2° S to 4° S and
211 west of 8° E in May-June (Fig. 1c). The orientation of surface current is mostly westward for the May-June
212 season, while it is northward from October to January (not shown). This general picture of surface circulation is
213 consistent with observations (Merle, 1972; Piton, 1988; Rouault et al., 2009).

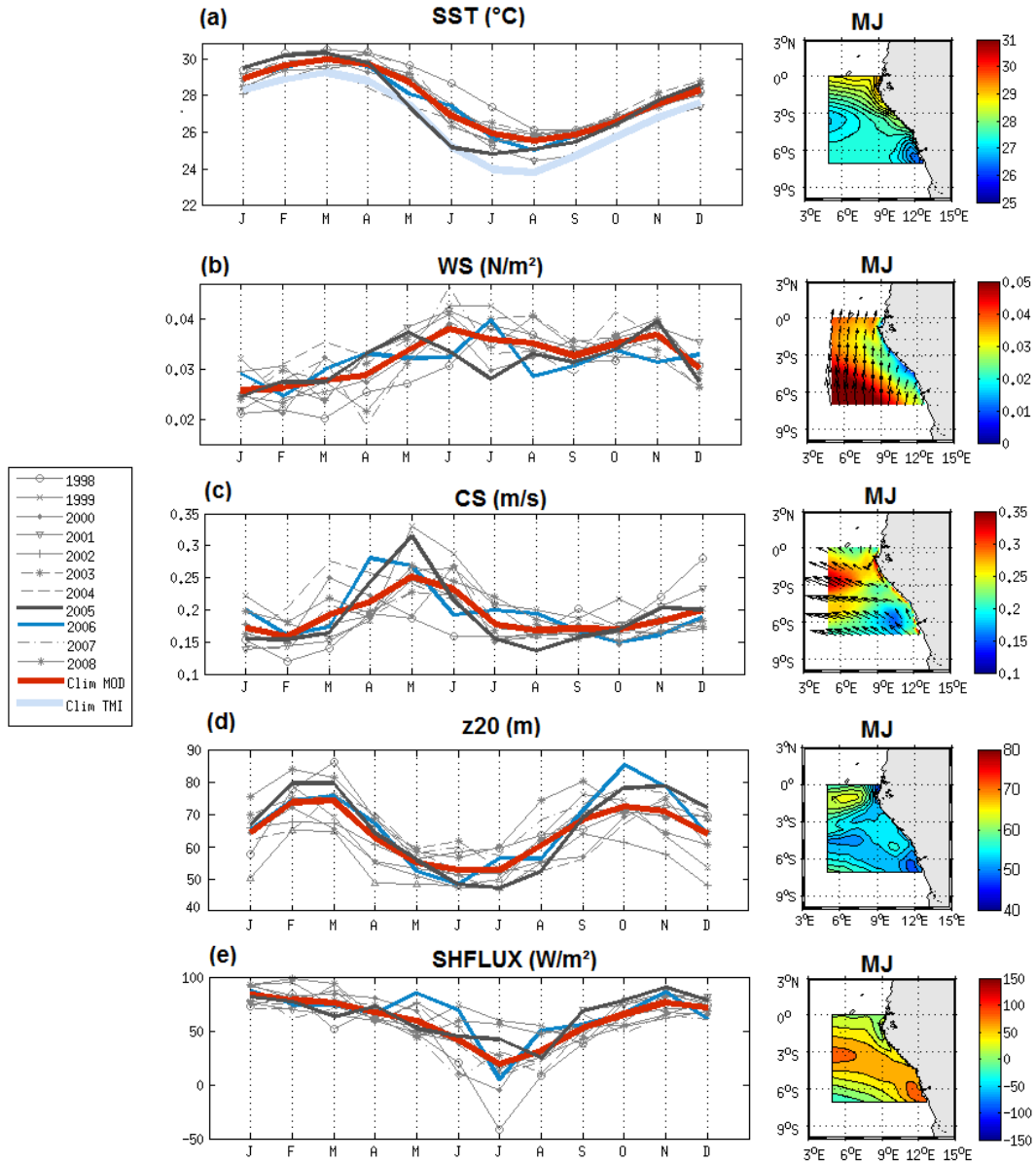
214 The region is also characterized by a shallow thermocline which depicts a strong semi-annual cycle (Fig. 1d).
215 The evolution of z20 reveals a shoaling of the thermocline during May-July and a deepening up to October-
216 November when it exhibits a maximum depth, in agreement with previous studies such as the one realized by
217 Schouten et al. (2005) who find a similar seasonal cycle from SSH altimetric data.

218 The surface net heat flux exhibits a maximum in boreal winter and a minimum in July (Fig. 1e), following the
219 seasonal cycle of solar shortwave radiations. As visible on the May-June average map, greater heating is found
220 over cool waters, due to weaker heat loss via latent heat flux in these areas.

221 The seasonal cycle is modulated by strong year-to-year variations. The mean SST in the CLR in 2005 cools as
222 early as March from TMI data and April from the model data. SST reaches weaker values than the climatologic
223 ones, as observed by Marin et al. (2009) and Caniaux et al. (2011) west of 4° E. This 2005 cold anomaly is
224 associated with positive wind speed and surface current speed anomaly in April-May (Fig. 1b&c) as well as
225 shallower-than-average thermocline depth. In 2006, SST variations are very close to the climatologic ones.

226

227 Thus, the April-June season in the CLR appears as a transitional period characterized by strong seasonal
228 evolution, primarily governed by the local winds which generate coastal upwelling in Congo mouth region and
229 modulated by the variation of thermocline depth.



230

231 **Figure 1:** Monthly average of the (a) sea surface temperature ($^{\circ}\text{C}$); (b) wind stress direction (vectors) and
 232 magnitude (color field) ($\text{N}\cdot\text{m}^{-2}$); (c) horizontal surface current direction (vectors) and speed (color field) ($\text{m}\cdot\text{s}^{-1}$);
 233 (d) 20°C -isotherm depth (m); and (e) surface heat flux ($\text{W}\cdot\text{m}^{-2}$; positive values indicate downward flux) from
 234 January to December from 1998 to 2008 and for the climatology (averaged over 1998-2008) simulated by the
 235 model (red curve) and from the observations : monthly average TMI 3-daily SST data (light blue curve in (a));
 236 averaged over 5°E - 14°E and 7°S - 0°S . Right panel: maps of each variable over May-June..

237

238 **4. Analysis of cooling episodes in the CLR in 2005 and 2006**

239 In this section, we examine the impact of intraseasonal wind bursts on SST in the CLR during the particular
240 years 2005 and 2006 (Marin et al., 2009; Caniaux et al., 2011). We propose here to analyze in details the SST
241 conditions in CLR, east of 5° E, for both years.

242

243

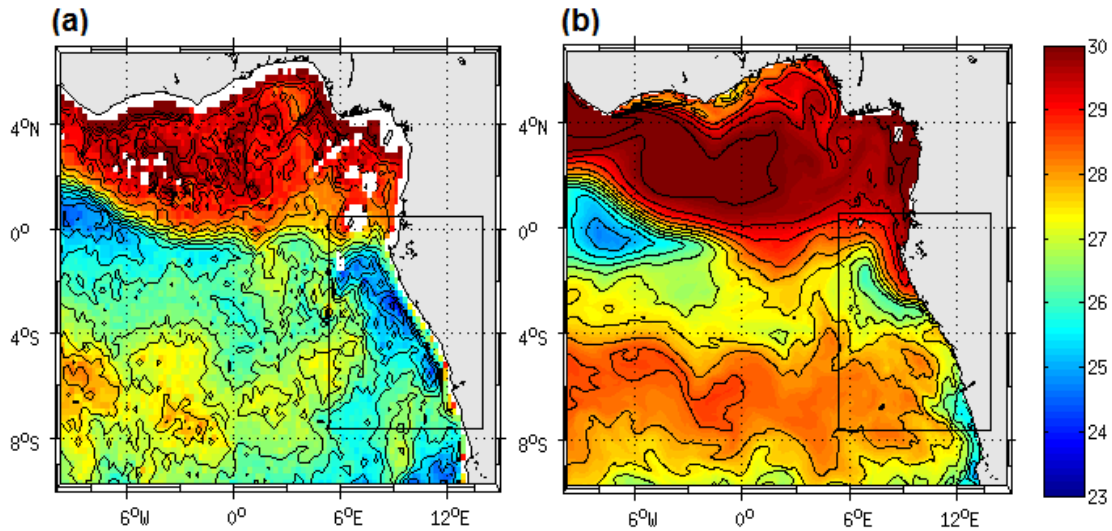
244 **4.1 SST variations**

245 In order to delineate the sequence of cooling episodes, we analyze the SST variations from 2-days averaged
246 model outputs in 2005 and 2006 over the CLR, i.e. between 5° E and 12° E. Both the SST (Fig. 3a & c) and
247 intraseasonal variations of SST (Fig. 4a & f) have been shown. In 2005, the intraseasonal cooling episodes took
248 place on 22-24 April, 8-12 May, 16-20 May, 26-30 May, 12-16 June and 30 June-2 July, with a temperature
249 drop ranging between -0.2°C to -1.7°C (Fig 4a). The cooling episodes occurred east of 5° E from May to
250 September. They concerned especially the southern equatorial region (around ~3-4° S), except for the strongest
251 events where they reached more northern equatorial regions, especially for the mid-May and late-May 2005
252 events. These latter were associated with an intense meridional SST front between the cold water south of the
253 equator and the warmer water north of the equator, as visible on SST map for 12 May 2005 presented on Fig. 2.
254 We can see cold waters extending along the eastern coast and in ACT region west of 5° W. In the model, cold
255 waters are deflected offshore off Cape-Lopez, due to recursive bias in warm water intrusion toward the south.

256 Besides, model SST fields (Fig. 3a) indicate that the SST minimum (~24° C) in 2005 was reached in July, i.e.
257 one month earlier than in 2006, as also noticed in seasonal variations of SST averaged in the region (Fig. 1a).
258 These results illustrate the important role of the succession of quick and intense cooling episodes in the
259 establishment of persistent cold anomalies in the CLR, as highlighted by Marin et al. (2009) in the equatorial
260 region.

261

262



263

264 **Figure 2:** Map of the sea surface temperature ($^{\circ}$ C) on 12 May 2005 from 3-days average TMI data (a) and from
 265 the 2-days average model output (b). Note that for the model it corresponds to 11-12 May average whereas for
 266 TMI data it is 10-11-12 May average. The black square indicates the Cape-Lopez region (called ‘CLR’).

267

268 4.2 Forcing mechanisms

269 4.2.1. Local forcing

270 To examine the local forcing mechanisms responsible for the observed cooling episodes in CLR, the
 271 intraseasonal variations of wind stress magnitude are examined and compared in 2005 and 2006 (Fig. 4b & 4g).
 272 In 2005, successive periods of 6-16 days wind intensification occurred from late-March to late-June. The main
 273 cooling episodes described above are associated with positive intraseasonal wind stress speed occurring on 4-6,
 274 12-16 & 24-28 May, and 10-12 & 28 June with a maximum for the 12-16 May event peaking on 14 May (at
 275 $\sim 0.025 \text{ N.m}^{-2}$). Another period of wind intensification is evidenced in late March – early April but it did not
 276 generate significant cooling despite comparable or even higher wind intensity than following wind events. In
 277 2006, periods of wind intensification extended from mid-March to July. The main wind events occurred in 14-
 278 16 March, 2-4 & 16-24 April, 4-6 & 12-18 May, 12-14 & 24-26 June and 10-12 July with maximum
 279 intraseasonal wind stress magnitude in 16-24 April (0.019 N.m^{-2}) and 24-26 June (0.022 N.m^{-2}). Also, the wind
 280 event in late April 2006 did not generate a surface cooling as strong as the mid-May 2006 one, despite higher
 281 wind stress magnitude. To depict the subsurface conditions during cooling episodes in the CLR for both years,
 282 the 20° C-isotherm depths averaged from 5° E to 12° E are presented on Fig. 3b & 3d. They indicate strong
 283 correlation with SST variations on intraseasonal time scale with minimum depths ($< 35 \text{ m}$) observed during the
 284 mid-May 2005 and end-May event. In early April 2005 and before the late-April 2006, the thermocline was
 285 deeper, that can explain why wind intensification did not generate a surface cooling at these times. Indeed, at the

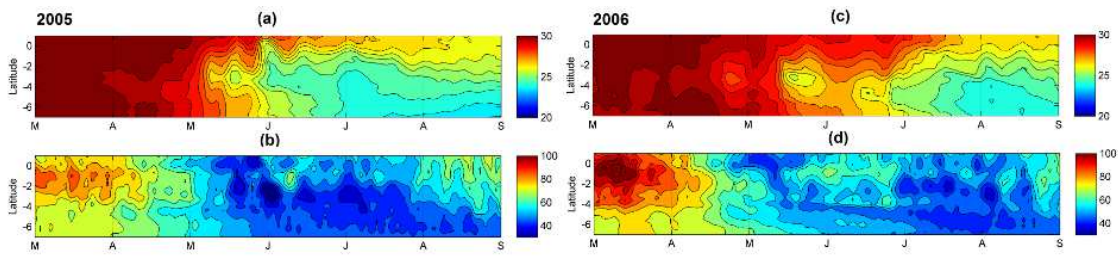
286 time of the strong 16-24 April 2006 wind event, the z_{20} values was higher south of the equator than during the
287 14-16 May 2005 event, making the SST less reactive to comparable wind intensification. The same feature is
288 observed in early May 2006, when the higher z_{20} values indicate deeper thermocline south of the equator
289 around 3-4° S than a few days later. Besides, the thermocline appeared globally shallower south of the equator
290 in 2005 than in 2006, in agreement with the difference of the cooling intensity observed between the two years.

291 The Ekman pumping velocity w_e averaged over the CLR for 2005 and 2006 is shown on Fig. 4d & 4i
292 respectively. The dates of intraseasonal upward velocities are quite well correlated with the dates of
293 intraseasonal wind events (with correlation coefficient equal to 0.55 for 2005 and 0.41 for 2006), maximum
294 being during the early-April, mid-May and end-May 2005 events and during .late April, mid-June and end-June
295 2006. However, for comparable wind intensification, the boreal spring and summer wind events were not
296 associated with comparable intensity of Ekman pumping velocity.

297 Another process that may contribute to the cooling in the upper layer is the vertical mixing due to intense
298 vertical shear of the current. The maximum of the vertical shear magnitude fields in the CLR, averaged between
299 5° and 12° E for 2005 and 2006 (Fig. 4c & 4h), exhibited intensification south of the equator, centered around 3-
300 4° S. Weaker intensification also occurred occasionally at the equator (located around 80 m depth between the
301 westward surface South Equatorial Current – SEC – and the eastward subsurface Equatorial Under- Current).
302 Around 3-4°S, the vertical shear was driven by the SEC, reinforced by prevailing southerly winds events
303 through Ekman transport. It thus occurred at the date of wind events previously identified for 2005 and 2006,
304 with stronger vertical shear occurring in early May 2005 and late April 2006. The intensity of the maximum of
305 vertical shear magnitude during the events was quite similar between 2005 and 2006. The main difference lied
306 in their meridional extent, related to the meridional extent of the strengthened southerly winds which reached
307 equatorial region during the May 2005 events (not shown). We can also notice that for comparable wind
308 intensification, the boreal spring and summer wind events were not associated with comparable intensity of
309 vertical shear. The meridional wind component favorable to westward Ekman transport was actually stronger
310 during April and May events than during summer ones (not shown).

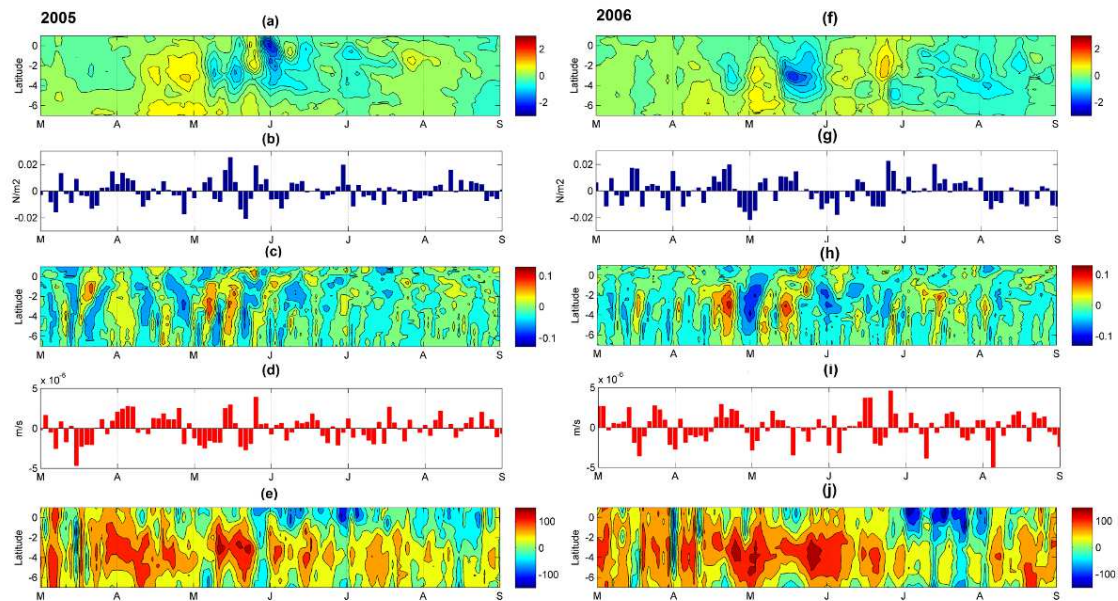
311 The heat content within the mixed layer is also impacted by the sea surface heat fluxes.
312 The net heat fluxes averaged between 5° E and 12° E are shown on Fig. 4e & 4j for 2005 and 2006 respectively.
313 They indicate a net heating ($\sim 50\text{-}100 \text{ W.m}^{-2}$) over the 2° S - 5° S latitude band, where the SST cooling was
314 strongest, suggesting other mechanisms involved. However, we notice some particular events during which the
315 net heat flux was negative over most of the region. A strong net cooling (-30 W.m^{-2}) occurred during the 26-28
316 May 2005 event. It was mainly due to a sudden decrease of incoming surface short wave radiation (drop of
317 about 80 W.m^{-2} in the CLR between 22 and 28 May; not shown) suggesting increased cloud cover. Another
318 strong net cooling occurred on 2 April 2006 with a mean value in the CLR reaching -95 W.m^{-2} . It is more sudden
319 than the end-May 2005's one, and was almost exclusively restricted to the CLR region with values reaching
320 locally -185 W.m^{-2} (not shown). For both events, the net cooling did not concern the equatorial region west of
321 0°W.

322



323

324 **Figure 3:** (a & c) Latitude-time diagram of the sea surface temperature (°C) averaged between 5°E and 12°E; (b
 325 & d) Latitude-time diagram of the 20° C-isotherm depth (m) averaged between 5° E and 12° E; from 1st March
 326 to 31 August 2005 (left panels) and 2006 (right panels).



327

328 **Figure 4:** (a & f) Time-latitude diagram, from 7° S to 1° N, of the intraseasonal variations of sea surface
 329 temperature (in ° C) averaged between 5° E and 12° E; (b & g) Time evolution of the intraseasonal variations of
 330 wind stress amplitude (N.m⁻²) averaged between 5° E and 12° E and between 3° S and 0° S; (c & h) Latitude-
 331 time diagram of the intraseasonal variations of the maximum of the current vertical shear magnitude (m.s⁻¹)
 332 averaged between 5° E and 12°E; (d & i) Longitude-time diagram of the intraseasonal variations of Ekman
 333 Pumping (m.s⁻¹) averaged over the CLR. Ekman pumping values >0 indicate upwelling; (e & j) Latitude-time
 334 diagram of the net heat flux (W.m⁻²) averaged between 5° E and 12° E; from 1st March to 31 August 2005 (left
 335 panels) and 2006 (right panels). For details about calculations of intraseasonal variations, see Sect. 2.

336

337

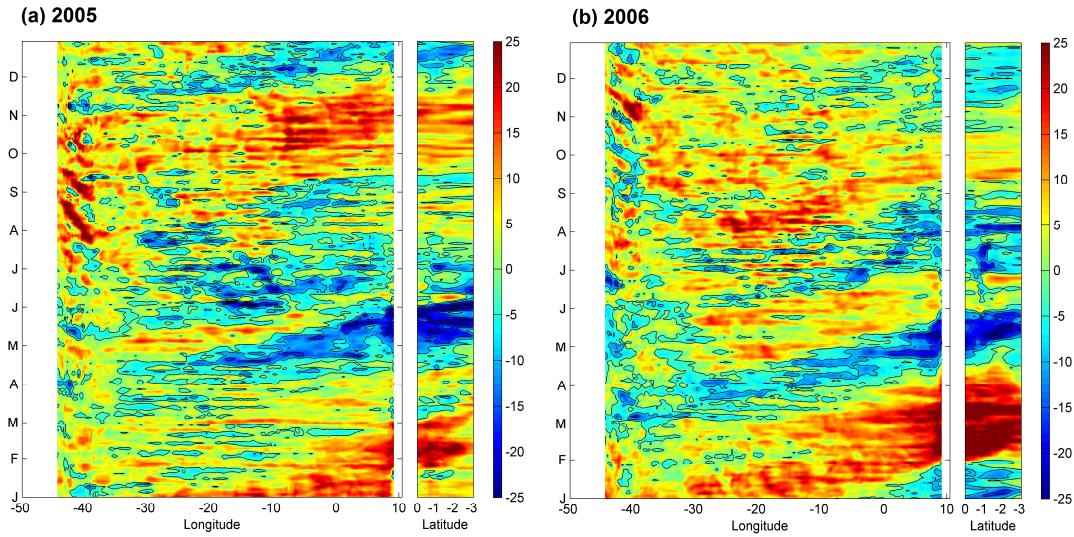
338 **4.2.2. Remote forcing**

339 **a. Highlighting of Kelvin wave propagation**

340 As previously shown, the time of occurrence of the cold events in the CLR coincides with shallow thermocline
341 which allows a mixed layer temperature to be more reactive to surface forcing. Indeed, because of its proximity
342 to the equator, the thermocline in the CLR is affected by the arrival of equatorial waves, initiated in the western
343 part of the basin. Pairs of alternate downwelling and upwelling Kelvin waves occur usually in February-March,
344 July-September and October-November. Upon impingement with the eastern boundary, the incoming equatorial
345 Kelvin wave excites westward-propagating Rossby waves and poleward-propagating coastal Kelvin waves
346 (Moore, 1968; Moore and Philander, 1977; Illig et al., 2004; Schouten et al., 2005; Polo et al., 2008). The 20°
347 C-isotherm depth anomalies along the equator and along 9°E are presented on Fig. 5 and clearly evidence large
348 negative anomalies indicating shallower-than-average thermocline, propagating eastward along the equator and
349 then southeastward for both years. The eastward propagation of Kelvin wave along the equator and
350 southeastward along the coast is also well visible in the basin-wide SSH anomalies (Fig. 6) with a phase
351 velocity of about 1.1-1.3m.s⁻¹, which fits well in the range between the second and third baroclinic equatorial
352 Kelvin wave modes. In 2005, negative SSH and z20 anomalies occurred in the West in early March- early April
353 and in mid-May, whereas they occurred around late-February – mid-March and early May and June in 2006.
354 The first Kelvin wave thus reached the CLR slightly earlier in 2006 than 2005, at the beginning of May. In
355 addition, the two upwelling Kelvin waves followed each other more closely in 2005 than in 2006.

356 Thus, the intensity of the cold events observed in boreal spring and summer 2005 and 2006 resulted from both
357 the basin preconditioning by remotely forced shoaling of the thermocline, local mixing and upwelling processes
358 in response to strong southerly local winds, as well as heat flux variations. In 2005, stronger wind intensification
359 and favorably preconditioned oceanic subsurface conditions, made the coupling between surface and subsurface
360 ocean processes more efficient than in 2006, resulting in stronger cooling.

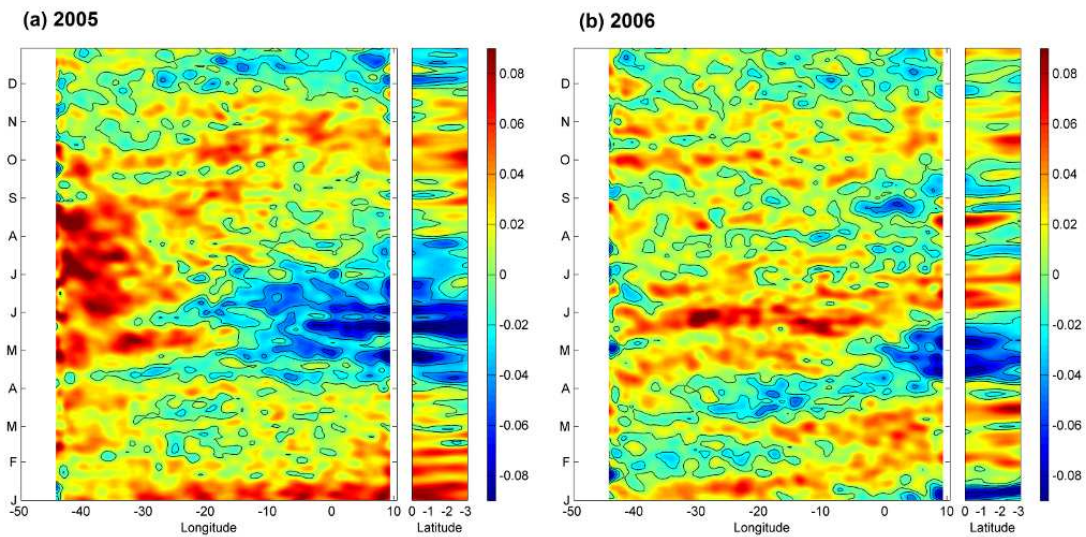
361



362

363 **Figure 5:** Time evolution of the intraseasonal anomaly of 20° C-isotherm depth (m) along the equator (between
 364 54° W and 12° E) and along 9° E (between the equator and 3° S) for 2005 (left) and 2006 (right). Negative
 365 values indicate a 20°C isotherm depth closer to the surface. For details about calculations of the anomalies, see
 366 Sect. 2.

367



368

369 **Figure 6:** Time evolution of the sea level anomaly (m) along the equator (between 54° W and 12° E) and along
 370 9° E (between the equator and 3° S) for 2005 (left), and 2006 (right) from AVISO data.

371

372

373 **b. Kelvin wave generation and coinciding atmospheric conditions in the West**

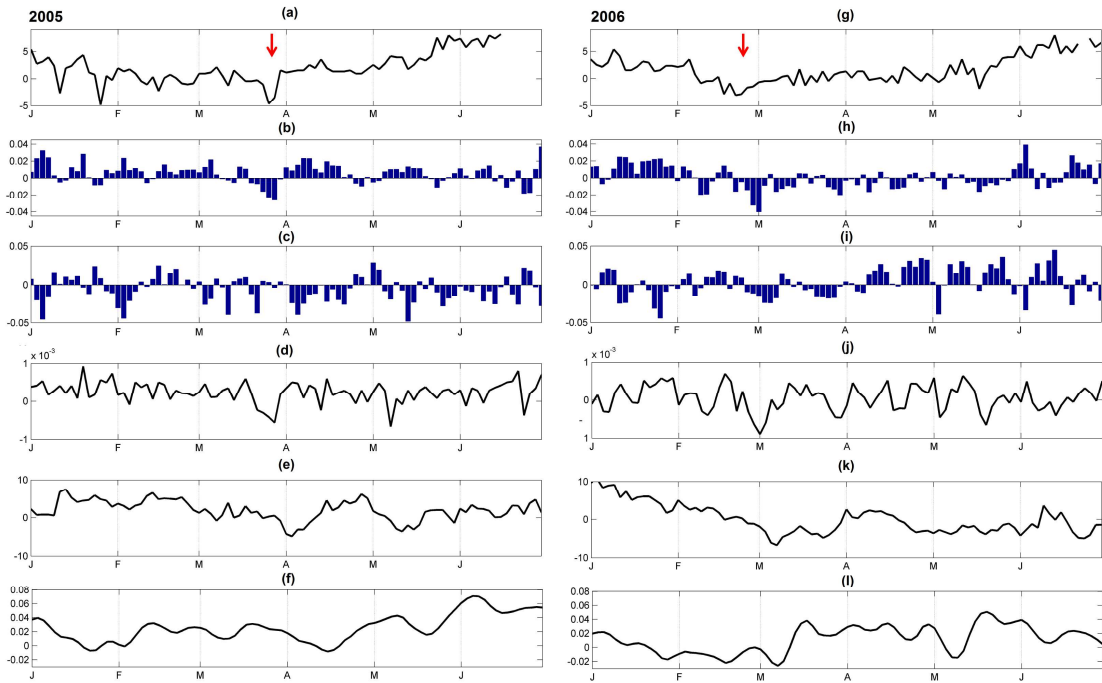
374 In order to identify the wind activity which accompanies the generation of Kelvin upwelling waves in winter
375 2005 and 2006 in the western part of the basin, we analyze the position of the ITCZ (averaged over 50° W-35°
376 W) identified as the latitude where the meridional wind stress goes to zero (Fig. 7a & g). The intraseasonal
377 anomaly of the zonal and meridional components of the wind stress (Fig. 7b-c & 7h-i), the intraseasonal
378 anomaly of wind stress curl (Fig. 7d & j), as well as the intraseasonal anomaly of the z20 and SSH (Fig. 7e-f &
379 k-l), averaged in the equatorial band (over 1° S and 1° N), are also presented. Many authors suggest that the
380 source of the equatorial Kelvin wave is mainly related to a sudden change of the western equatorial zonal wind
381 (e.g. Picaut, 1983; Philander, 1990): a symmetric westerly (easterly) wind burst along the equator will generate
382 Ekman convergence (divergence) and thus force downwelling (upwelling) anomalies which then propagate
383 eastward as a Kelvin wave (Battisti, 1988; Giese and Harrison, 1990). In 2005, shallower-than-average
384 thermocline, evidenced by negative z20 and SSH anomalies, occurred in the end of March-beginning of April in
385 the west part of the basin (Fig. 7e & f). The intraseasonal anomalies of meridional and zonal wind stress indicate
386 that the maximum of thermocline slope anomaly was associated with a strengthening of northeast trades
387 followed by a strengthening of southeast trades from either side on the equator. At the equator, we notice indeed
388 a sudden reversing of meridional winds which turned southward on 27-28 March 2005 related to an abrupt
389 southward displacement of the ITCZ which was then found south of the equator in the west part of the basin
390 (Fig. 7a & b). The ITCZ returned its initial position four days later followed by a strengthening of easterlies
391 which persisted for ~20 days (Fig. 7c). Climatologically, the latitudinal position of the ITCZ varies from a
392 minimum close to the equator in boreal spring (March-May) in the west to a maximum extension of 10°N –
393 15°N in late boreal summer (August) in the east. Positive (negative) wind stress curl is found north (south) of the
394 ITCZ. When the ITCZ is north of the equator, it induces upward (downward) Ekman pumping to the north
395 (south) of the ITCZ. Thus, the southward shift of the ITCZ on 27-28 March 2005 accompanied with strong
396 northerlies led to negative anomaly of wind stress curl south of the equator resulting in upward Ekman pumping.
397 Results show indeed a strong negative anomaly on 22-26 March 2005 associated with the southward shift of the
398 ITCZ just before the upwelling signal, initiated on 28 March. These changes contributed to a rise in the oceanic
399 thermocline with a time lag of some days (Fig. 7e & f). The upwelling signal might then be reinforced by the
400 symmetric easterly wind which concerned a large part of the western basin. Besides, we identify on Fig. 7d
401 another peak of negative wind stress curl anomaly on 6-8 May 2005, more sudden than the previous winter one.
402 It was associated with negative z20 SSH anomalies indicator of a thermocline rise initiated on 6 May 2005 in
403 the west of the basin and which propagated eastward along the equator. The zonal wind stress anomalies (Fig.
404 7c) also indicate an easterly wind strengthening initiated in the beginning of May, which a maximum on 8-10
405 May, just after the minimum of wind stress curl.

406 In 2006, the upwelling Kelvin wave is identified in the first half of March in the west part of the basin (Fig. 7k
407 & l). The coinciding atmospheric conditions were slightly different than the ones identified in 2005. In winter,
408 the position of the ITCZ had a more southern position in 2006 than in 2005. It crossed the equator during a
409 longer period (about 10 days from ~ Feb. 10 2006), reaching minimum latitude on 22-24 February. This location

410 south of the equator induced a negative wind stress curl anomaly (Fig. 7j). As in 2005, the reversion of the
 411 meridional wind at the equator was followed by a strengthening of westward component of the wind stress few
 412 days after, which lasted for about ten days (Fig. 7i); however, it was of a lesser magnitude compared to 2005
 413 and only concerned the westernmost part of the basin. In addition, the negative zonal wind anomaly concerned
 414 mainly the northeasterlies rather than the southeasterlies, leading to an anti-symmetric meridional wind pattern as
 415 well as symmetric zonal wind pattern on either side on the equator (not shown). These wind patterns were
 416 expected to generate Ekman convergence at the Equator and thus to reinforce the observed upwelling anomalies.

417

418 Thus, for both years, Kelvin upwelling wave occurred in the west while easterly winds were strengthened from
 419 either side of the equator after the ITCZ reached its southernmost location. This latter was observed one month
 420 earlier in 2006 than in 2005, and was associated with a negative wind stress curl anomaly. In winter 2005, the
 421 ITCZ was found south of the equator after a very sudden southward shift and was followed by strong easterlies
 422 during ~20 days, while in winter 2006, the ITCZ was found closer to the equator less sharply and during a
 423 longer period, followed by weaker easterlies compared to 2005. These results highlight another way in which
 424 wind intraseasonal events may impact the SST variability in the East part of the basin, through the generation of
 425 Kelvin wave in the West which shoals the thermocline in the East few weeks later.



426

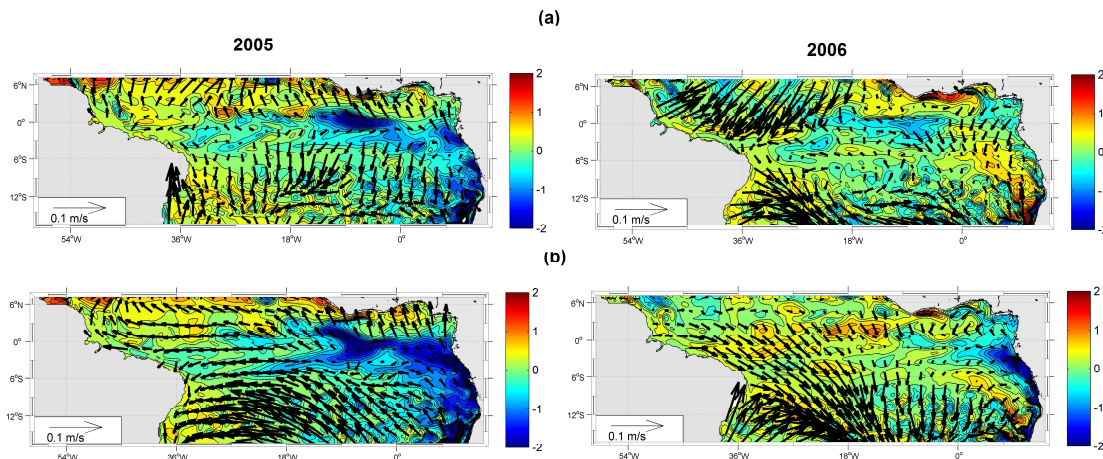
427 Figure 7: Time evolution, from 2-days averaged model outputs over Jan-June2005 (left) and Jan-June 2006
 428 (right); of (a & g) the position (in latitude, between 5° S and 10° N) where the meridional wind stress value
 429 equal zero (indicator of the position of the ITCZ); (b & h) the intraseasonal anomaly of the meridional wind
 430 stress ($N.m^{-2}$) averaged between 50° W and 35° W and between 1° S and 1° N; (c & i) same as (b & h) but for

431 intraseasonal anomaly of zonal wind stress ($N.m^{-2}$); (d & j) the intraseasonal anomaly of the wind stress curl
 432 ($N.m^{-2}$); (e & k) the intraseasonal anomaly of the $20^{\circ}C$ isotherm depth (m); (f & l) the intraseasonal anomaly of
 433 the sea level (m). The red arrow in (a & g) indicates the southward shift of the ITCZ before the generation of the
 434 Kevin wave (see text). For details about the calculations of anomalies, see Sect. 2.

435

436 4.3. Westward extension of the CLR cooling

437 In the east, the cooling generated by southerly wind bursts in the CLR then progressively extended westward to
 438 connect with the southern boundary of the equatorial ACT. This phenomenon was more obvious in 2005 when
 439 the cooling which first concerned coastal area extended further offshore a few days after the two strong events
 440 occurring in the second half of May. To evidence the effect of these events on SST, maps of intraseasonal SST
 441 anomaly and intraseasonal wind stress anomaly averaged from 1 to 12 May (before the strong 2005 events; Fig.
 442 8a) and from 14 to 31 May (during and after the strong 2005 events; Fig. 8b) are presented on Fig. 8. The same
 443 calculations have been for 2006 for comparison. The results illustrate an enhancement after 10 May of the
 444 cooling in the east associated with southerly wind intensification and an extension of the cooling especially
 445 south of the equator up to $20^{\circ}W$.



446

447 **Figure 8:** (a) intraseasonal anomaly of sea surface temperature ($^{\circ}C$; color) superimposed with intraseasonal
 448 anomaly of wind stress intensity (arrows) averaged over 1-12 May 2005 (up panel) and over 14-30May (down
 449 panel); (b) same but for 2006. For details about the calculations of the anomalies, see Sect.2.

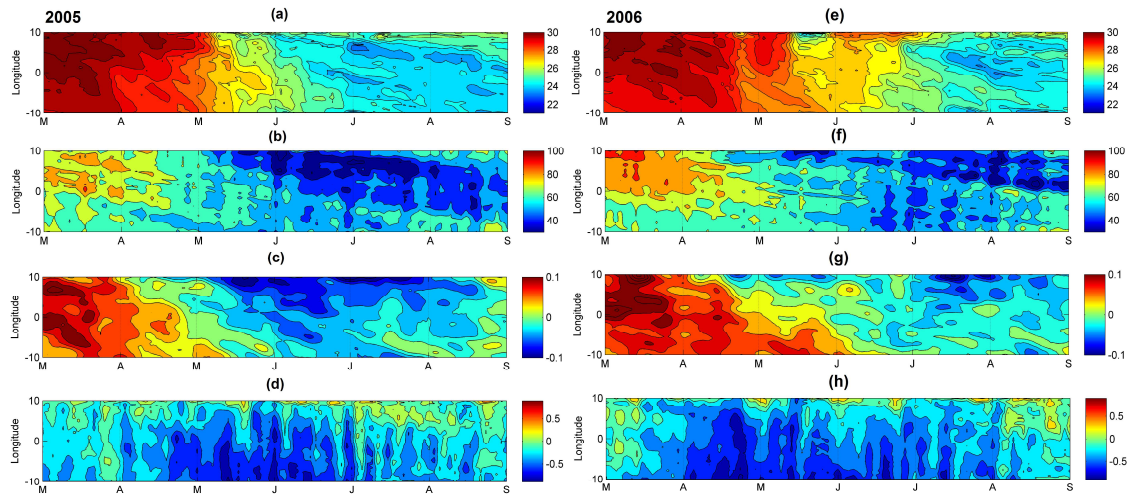
450 To better understand the oceanic processes implied in this cooling extension, we compared the SST, z_{20} , SLA
 451 and zonal velocities along $3^{\circ}S$ from March to September 2005 (Fig. 9 a-d) and 2006 (Fig. 9 e-h). In 2005, the
 452 cooling westward extension was associated with a westward propagation of a shallower thermocline and
 453 negative SLA from the African coast up to $5^{\circ}-10^{\circ}W$ combined with enhanced surface westward current
 454 fluctuations at the dates of the successive events from April-June. The fluctuations of the westward surface

455 current occurring off Gabon with periods of ~8-10 days were related to the strengthening of southerly winds
456 during the wind bursts at the same periods (Fig. 4b & g). The surface current in this area is part of the westward
457 SEC which is known to intensify during the cold season (Okumura and Xie, 2006). Our study implies shorter
458 time scales than seasonal scale but the intensification of the SEC during wind bursts through Ekman transport
459 processes might contribute to the westward extension of the cooling by advection of cold eastern upwelled
460 water. This is in agreement with DeCoëtlogon et al. (2010) who found from model results that at short time
461 scale (a few days), more than half of the cold SST anomaly around the equatorial cooling could be explained by
462 horizontal oceanic advection controlled by the wind with a lag of a few days. In addition, minimum z20 and
463 SLA values propagating westward at 3° S (Fig. 9b & c), initiated from the coast with a propagating speed of
464 around 10 cm.s⁻¹, which is very close to the phase speed of Rossby waves. Indeed, the generation of the
465 westward waves at the coast coincided with the arrival of Kelvin waves (see Fig. 5a) suggesting the possibility
466 of Kelvin wave's reflection processes into symmetrical westward propagating Rossby waves. A westward
467 propagation of z20 and SLA minimums, although less obvious, was presently also identified at 3° N (not
468 shown).

469 In 2005, the locally wind-forced component of the wave might reinforce the remote part of the reflected wave
470 signal at the coast by the sea level slope which balanced the strengthening of alongshore winds blowing during
471 the mid-May and late-May events. The quantitative and respective contributions of local and remote wind
472 forcing to this wave is out of the scope of this study and would require further analysis. This phenomenon is
473 supported in 2005 by anomalous eastward expanded southerly wind bursts observed in May 2005. The month of
474 May is besides a period when westward surface currents are usually maximum (as visible on the mean seasonal
475 cycle shown on Fig.1c). Thus, the combined effects of westward surface currents (via advection and vertical
476 mixing through horizontal current vertical shear), local wind influences (via vertical mixing) and wave
477 westward propagation, resulted in the extension of cold upwelled water from the eastern coast to near 20° W.

478 In 2006, the westward extension of cold waters established later, from the beginning of July. A coastal cooling
479 occurred on 18-26 May but no westward extension of the cold waters is observed at this period (Fig. 9e). In
480 2005, the two upwelling Kelvin waves followed each other closely while in 2006, the first Kelvin upwelling
481 wave reached the coast in May and the second in July (Fig.5b & Fig. 6b and Fig. 9f). In addition, the
482 intraseasonal wind strengthening responsible of the coastal cooling on 18-26 May 2006 is less intense (wind
483 stress mean in the CLR ~0.04N.m²) than the one in mid-May 2005 (~0.06N.m²; which is preceded and followed
484 by another wind bursts few days before and after; Fig. 3b & Fig. 4b).

485 The analysis over 1998-2008 period shows that the westward extension of the cold SST takes place every year
486 but begins at different times of the year (not shown). It occurs generally from June-July, when the cooling
487 events usually occur in the east at this location, and is thus closely linked with the shoaling of the thermocline
488 due to the arrival of a Kelvin upwelling wave at the eastern coast



489

490 **Figure 9:** Time-longitude diagrams at 3° S between 10° W and 10° E, and from 2-days averaged model outputs from 1st
 491 March to 31 August 2005 and 2006, of (a & e) the sea surface temperature (° C); (b & f) the 20° C isotherm-depth (m); (c &
 492 g) the sea level anomalies from AVISO data (m); and (d & h) the zonal component of surface velocity (m.s⁻¹).

493

494 In conclusion to this section 4, the SST variability in the CLR at intraseasonal time scales is the result of
 495 combination between basin preconditioning by remotely forced shoaling of the thermocline via Kelvin wave,
 496 local mixing induced by current vertical shear, and upwelling processes in response to strong southerly winds.
 497 As highlighted for the 26-28 May 2005 and 2 April 2006 events, the net heat flux may also contribute to cool
 498 the surface waters, through enhanced cloud cover which decrease the incoming solar radiation. The cold
 499 upwelled waters around 3°S extend then westward from the eastern coast to near 20°W by combined effect of
 500 the westward propagating Rossby waves as well as vertical mixing and advection processes. The cool water may
 501 thus contribute to the cooling in the southern edge of the cold tongue region. Although the processes implied
 502 differ slightly due to the presence of the coast, the SST variability in the CLR is quite close to the one in the
 503 equatorial cold tongue region (not shown), due to similar atmospheric forcing. However, for a given wind burst,
 504 the intensity of SST response in the CLR and in the cold tongue region is modulated by subsurface conditions
 505 which are under the influence of equatorial Kelvin wave. In May 2005, the Kelvin wave reached the eastern
 506 coast while three wind bursts occurred. The thermocline was thus shallower in the east than west of 0°W,
 507 providing favorable subsurface conditions making the coupling between making the SST more reactive to wind
 508 intensification occurred during this month. In addition, the decrease short wave radiations due to enhanced cloud
 509 cover during the 26-28 May 2005 event or 2 April 2006 event, which contribute to the cooling in the CLR, did
 510 not concern the equatorial region east of 0°W.

511

512

513 **5. Focus on the mid-May 2005 event**

514 We have previously identified five main cold events in 2005 (22-24 April, 8-12 May, 16-20 May, 26-30 May
515 and 14-18 June), characterized by a temperature drop ranging from -0.2°C to -1.7°C in the model. Analysis of
516 intraseasonal wind stress magnitude (Fig. 4b) has revealed that each event is associated with strengthening of
517 equatorward winds, especially during the 14-16 May event when the intraseasonal wind stress magnitude
518 averaged over the CLR is the strongest one. This particular event has been found to be responsible for the
519 sudden and intense SST cooling in the eastern equatorial Atlantic and identified as part of manifestation of
520 temporal variability of the St. Helena Anticyclone (Marin et al., 2009). In this section, we focus on this mid-
521 May event, to better understand the processes at play during this unusual event.

522

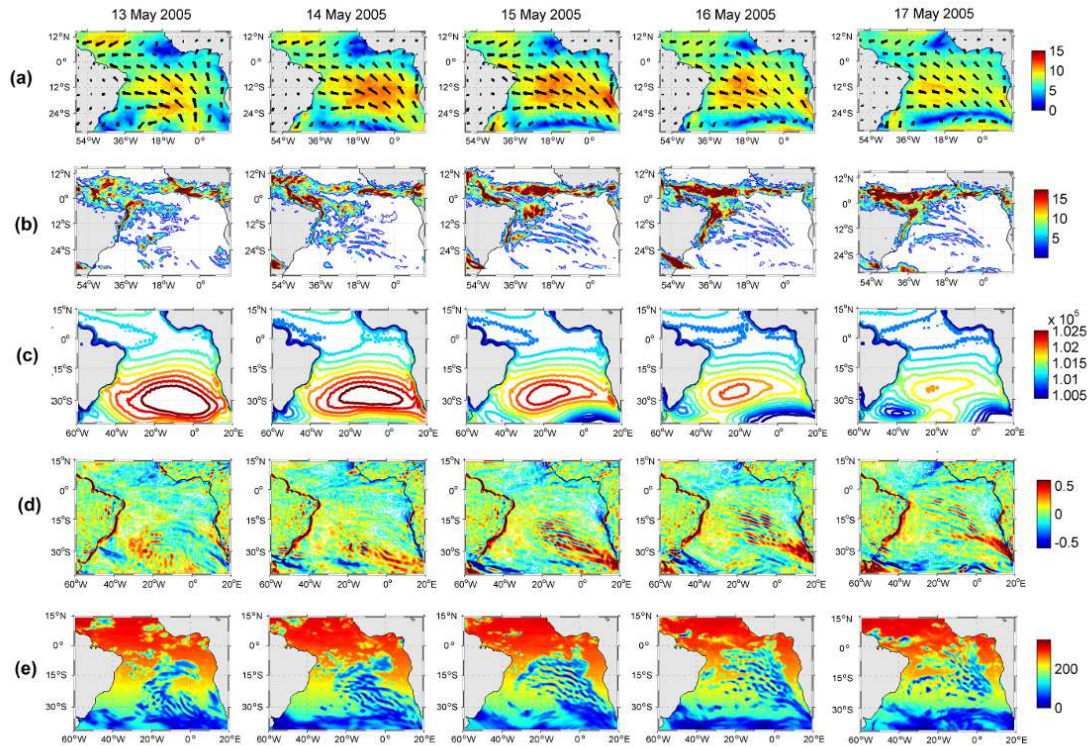
523 **5.1 Atmospheric conditions**

524

525 **5.1.1 Wind and surface atmospheric pressure**

526 The spatial distribution of the mid-May 2005 wind event can be inferred from Fig. 10 where CFSR wind speed
527 fields superimposed with daily precipitation fields, surface pressure, wind speed curl, and downward shortwave
528 radiation, are presented from 13 May to 17 May. The event was characterized by intense southeasterly wind east
529 of 15°W and from 30°S to the equator from 13-14 May, concomitant with a strengthening of the easterlies west
530 of 30°W between 30° and 15°S (Fig. 10a). The strong southeasterly winds drifted then westward up to 15-16
531 May when the maximum was located in the western part of the basin off northeastern Brazilian coast.
532 Simultaneously, a strengthening of southerly winds occurred north of the equator in the Gulf of Guinea. The
533 strong winds during the event were associated with high pressure core of the Saint Helena Anticyclone,
534 especially on 13-14 May, also associated with particularly low pressure under the ITCZ 4 days later (Fig. 10c).
535 The pressure fall during the mid-May 2005 event appeared as the lowest in May over the whole decade (not
536 shown). The meridional surface pressure gradient during the event is thus found to be the strongest over 1998-
537 2008 period. That suggests strong Hadley circulation intensity during the mid-May event and therefore strong
538 equatorward moisture flux, allowing the deep atmospheric convection in the Gulf of Guinea to be triggered at a
539 self-sustaining level (see Sect. 5.2 following).

540



541

542 **Figure 10:** Daily-averaged, from 13 May to 17 May 2005 (left to right panels), of (a) wind magnitude (color
 543 field) (m.s^{-1}) superimposed with wind vectors from CFSR fields; (b) precipitation rate ($\text{kg.m}^{-2}/\text{day}^{-1}$) from
 544 CFSR fields; (b) surface pressure (hPa) from ERA-20C reanalysis; (c) wind speed curl (m.s^{-1}) computed from
 545 CFSR wind speed fields; and (d) downward short-wave radiation (W.m^{-2}) from CFSR fields.

546

547 5.1.2 Precipitation

548

549 The maps of precipitation rate during the event (Fig. 10b) display a band of heavy precipitation ($9\text{-}17 \text{ kg.m}^{-2}/\text{day}$)
 550 $^2/\text{day}$) between $5^\circ - 9^\circ \text{ N}$ and off northeast Brazil from the coast to 15° W and from 10° S to 3° S . The maximum
 551 precipitation rate in this region occurred on 15-16 May concomitant with the easterly winds strengthening. This
 552 convective zone, located between the ITCZ north of the equator and the South Atlantic Convergence Zone
 553 (SACZ) in southern tropics, is the Southern Intertropical Convergence Zone (SICZ) (Grotsky and Carton,
 554 2003). This zone forms usually later, by June-August, when the southern branch of the convection separates
 555 from the ITCZ which moves north of the equator. Grotsky and Carton (2003) showed that this rainfall pattern
 556 appears closely linked to the seasonal change in SST difference between the ACT region (which they defined
 557 between $15^\circ \text{ W} - 5^\circ \text{ W}$, $2^\circ \text{ S} - 2^\circ \text{ N}$) and the SITCZ region ($25^\circ \text{ W} - 20^\circ \text{ W}$, $10^\circ \text{ S} - 3^\circ \text{ S}$). They argued that the
 558 seasonal appearance of the ACT along the equator sets up pressure gradients within the boundary layer that
 559 induce wind convergence in the SITCZ region. Based on Grotsky and Carton (2003) results, the unusually

560 rainfall conditions during mid-May event might thus be explained by strong SST gradient between the two
561 regions caused by unusually early cooling in the ACT region at this time of the year.

562

563 **5.1.3 Generation of atmospheric gravity wave**

564

565 The precipitation fields during the mid-May event (Fig. 10b) also evidence rainfall pattern typical of
566 atmospheric gravity wave train characterized by a horizontal wave length ~ 500 km and initiated by a front
567 system (forming the northern boundary of a low pressure system) which developed around 17° S on 14 May and
568 traveled northeastward until 17 May. The rainfall train was associated with oscillatory wind speed curl train
569 alternating between positive and negative values (Fig. 10d) as well as alternating downward shortwave radiation
570 minimum (Fig. 10e) associated with the wave clouds. Gravity waves are known to play an important role in
571 transporting the momentum and energy through long distances (Fritts, 1984). Here, they would be a way to
572 carry momentum and energy from South Atlantic to the equator during the strong event.

573

574 **5.2 A decisive event for coastal monsoon onset**

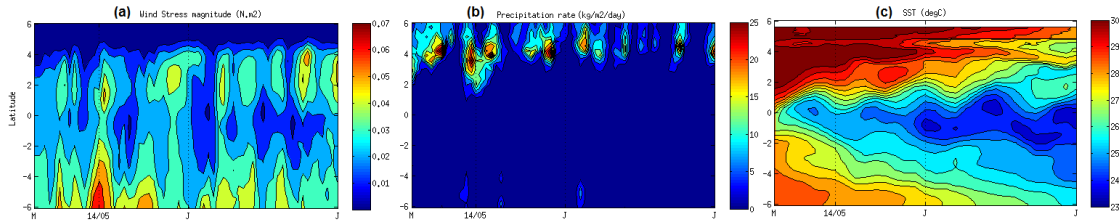
575 The mid-May 2005 wind event was found to be involved in the early onset of the ACT development (Marin et
576 al. 2009, Caniaux et al., 2011). The influence of the cold tongue on the WAM onset has been suggested by
577 several authors (Okumura and Xie, 2004; Caniaux et al., 2011; Nguyen et al., 2011; Thorncroft et al., 2011). At
578 the seasonal time-scale, Caniaux et al. (2011) suggest that it comes from strong interactions between the SST
579 cooling and wind pattern in the eastern equatorial Atlantic: the ACT serves to accelerate (decelerate) winds in
580 the northern (southern) hemisphere contributing to the northward migration of humidify and convection, and
581 pushes precipitation to the continent. Thus, due to its impact on ACT development, the mid-May 2005 wind
582 event is also linked to the onset of the WAM in 2005 which has been the earliest over 1982-2007 period from
583 Caniaux et al. (2011). In this section we aim to better understand how this single wind event may have such
584 impact. For further information on the WAM, the reader can refer to Leduc-Leballeur et al. (2013) and Caniaux
585 et al. (2011).

586

587 In order to analyze the air-sea pattern in the northern Gulf of Guinea during May-June 2005, we show in Fig. 11
588 the wind stress magnitude, precipitation rate, and SST fields averaged from 10° W to 6° W. The wind
589 strengthening appeared first south of the equator on 12-16 May and then north of the equator from 14-18 May. It
590 was associated with strong rainfall extending southward up to 2° N. Equatorial cooling occurred 4 days after
591 the event and slowed down the overlying winds by feedback mechanisms. The winds north of the equator then
592 remained stronger than in the ACT region and strengthened again north of the Equator on 22-28 May together
593 with precipitation maximum pushed northward (around 5° N) after the event.

594 Thus, this mid-May event appears as the “decisive event” which triggered the abrupt transition between the two
595 wind patterns in the northern Gulf of Guinea, when the wind north of the equator became and remained stronger

606 than south of the equator. It occurred 15 days earlier than the average date (31 May) identified by Leduc-
 607 Leballeur et al. (2013) over 2000-2009 period. According to these authors, the time of occurrence of this
 608 phenomenon would be related with the strength of anomalous moisture flux. They explain that in April-May the
 609 low atmospheric local circulation is present only during an equatorial SST cooling and surface wind
 610 strengthening north of the equator, both generated by a southerly wind burst, before disappearing until the next
 611 wind burst. In June-July the low atmospheric local circulation is then always present and intensified by the wind
 612 bursts. Thus, the establishment of an abrupt seasonal transition event as observed in 2005, occurring much
 613 earlier than the reference date, supposed anomalously strong equatorial cooling caused by unusual strong
 614 southerly winds which allowed, through air-sea interactions mechanisms, to trigger the deep atmospheric
 615 convection in the Gulf of Guinea at a self sustaining level.



607
 608 **Figure 11:** Time evolution, in May and June 2005 between 6° S and 6° N and averaged between 10° W and 6°
 609 W, of the (a) daily averaged wind stress magnitude ($N.m^{-2}$) computed from CFSR wind speed fields ; (b) daily
 610 averaged precipitation rate ($kg.m^{-2}/day$) from CFSR fields and (c) 2-daily averaged SST ($^{\circ}C$) fields, from the
 611 forced model.

612

613 **5.3. Why made the mid-May 2005 event so special?**

614

615 To better understand which makes the particularity of the mid-May 2005 event, the atmospheric and oceanic
 616 conditions (SST, intraseasonal SST anomalies, intraseasonal short-wave radiation flux anomalies (hereafter
 617 RADSW), intraseasonal wind stress magnitude anomalies, intraseasonal z20 anomalies, and intraseasonal
 618 meridional SST gradient anomalies) averaged over the 10° W - 6° W region and between 15° S to 5° N during
 619 April-May are analyzed over the 1998-2008 period (Fig. 12). The intraseasonal wind stress magnitude anomaly
 620 during mid-May event appears to be one of the strongest over the whole 1998-2008 period (up to $0.13N.m^{-2}$
 621 around 15°S and $0.05N.m^{-2}$ in equatorial region). These strong wind conditions are usually met later in late
 622 boreal spring or summer, when the St. Helena Anticyclone strengthens and shifts northward toward the warm
 623 hemisphere. The wind intensification in mid-May 2005 was associated with particularly weak RADSW from
 624 South Atlantic to the northern equatorial region, suggesting cloud albedo effect during the event which tended to
 625 cool the mixed layer. We can notice that the April-May 2005 period was characterized by the weakest mean
 626 RADSW.

627 In addition, at the time of the event, the surface waters were already cooled by previous wind bursts (e.g. 20
 628 April and 8 May). The SST response to the mid-May event occurred 4-6 days later, inducing the weakest

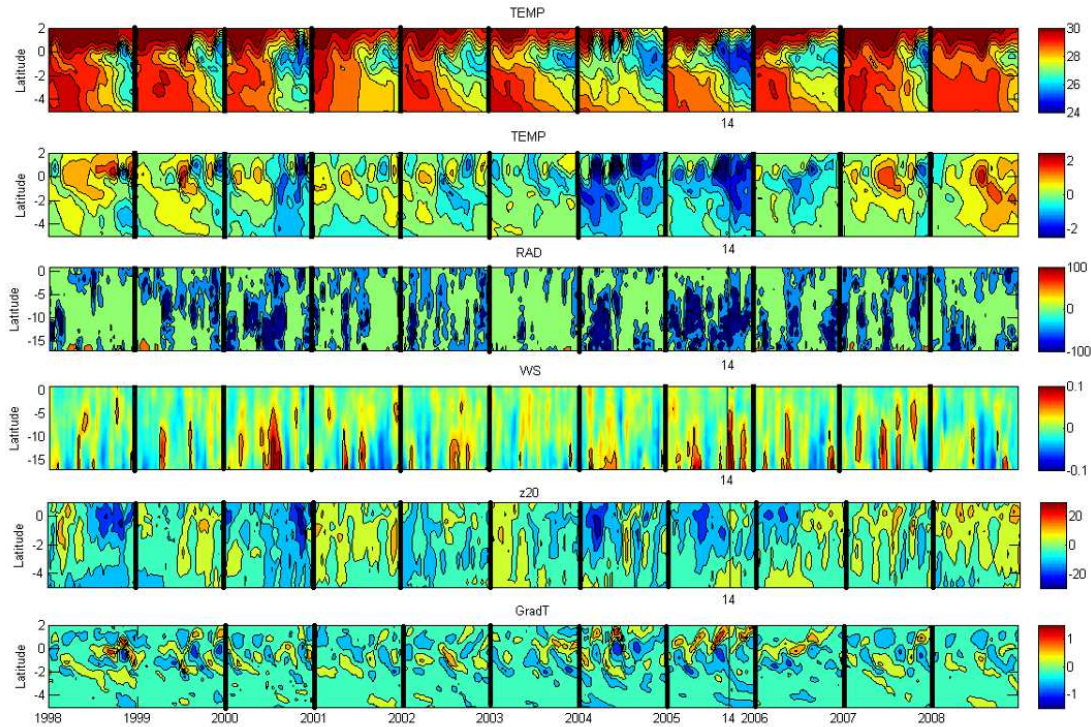
629 equatorial SST values for April-May season over the whole 1998-2008 period (SST drop of $\sim 3^{\circ}\text{C}$ inducing SST
630 $< 24.8^{\circ}\text{C}$). The cooling also caused an enhanced SST front around 1°N , as shown on Fig. 12 (bottom panel),
631 which was found to be the earliest and strongest one over the 1998-2008 period. This meridional SST gradient
632 was responsible for the wind surface intensification north of the equator (Fig. 11a and Fig. 12, fourth panel)
633 through air-sea interaction mechanisms as described by Leduc-Leballeur et al. (2011). Another SST gradient
634 maximum is found at the end of May 1998 but it was not extended as eastward than during the mid-May 2005
635 event (not shown).

636 When the wind burst occurred on 14 May 2005, the 20°C -isotherm depth in the area was anomalously shallow
637 south of the equator and slightly deeper at the equator (Fig. 12, fifth panel). The thermocline shoaling associated
638 with the Kelvin wave appeared in fact a few days earlier providing favorable subsurface conditions which made
639 the SST response to previous wind bursts (20 April and 8 May) more effective. At the time of the mid-May
640 event, the wave already reached more eastern areas, as shown in previous sections.

641

642 Thus, the particularity of the mid-May 2005 event mainly lies in the i) anomalous atmospheric conditions
643 related to strong St. Helena Anticyclone perturbation; ii) cooling initiated by the succession of previous wind
644 bursts; and iii) favorable subsurface local ocean conditions preconditioned by equatorial waves which shoaled
645 the mixed layer. Another wind burst of comparable intensity occurred at the beginning of May 2000 (Fig. 12,
646 fourth panel) while the thermocline was shallow, causing SST cooling at the equator (Fig. 12, first and second
647 panels). However, the wind strengthening was less sudden than during the mid-May 2005 event and the
648 resulting cooling took place over a less broad region (not shown). In addition, the surface pressure drop in the
649 ITCZ region was not as pronounced as during mid-May 2005 event.

650



651

652 **Figure 12:** Time-latitude diagrams for April-May along the 1998-2008 period, of 2-days average, from top to
 653 bottom i) SST ($^{\circ}C$); ii) intraseasonal anomaly of SST ($^{\circ}C$); , iii) intraseasonal anomaly of wind stress
 654 magnitude ($N.m^{-2}$) from CFSR fields; iv) intraseasonal anomaly of short-wave radiation surface flux ($W.m^{-2}$)
 655 from CFSR fields; v) intraseasonal anomaly of 20 $^{\circ}C$ -isotherm depth (m) computed from the forced model SST;
 656 vi) intraseasonal anomaly of meridional SST gradient (every 0.5 $^{\circ}$ of latitude), from the forced model; averaged
 657 over 10 $^{\circ}$ W-6 $^{\circ}$ W. The vertical black thin line indicates the date of 14 May, 2005. For details about the
 658 calculations of the anomalies, see Sect. 2.

659

660 6. Summary and discussion

661 In this study, the impact of intraseasonal winds on SST in the far eastern Tropical Atlantic during boreal spring
 662 2005 and 2006 has been investigated from observations and numerical simulation. We first focus our study in
 663 the Cape-Lopez region (CLR), east of 5 $^{\circ}E$ and between the equator and 7 $^{\circ}$ S, where the seasonal and interannual
 664 SST variability is poorly documented. There, the boreal spring (AMJ) season corresponds to a transitional
 665 period between high SST in boreal winter and weak SST in boreal summer, under the influence of local winds.
 666 Intensified cool SSTs are observed in the coastal upwelling area located around 6 $^{\circ}$ S in the Congo mouth region,
 667 associated with mean alongshore wind conditions. Boreal spring season is in fact characterized by maximum
 668 winds amplitude, influence of which is made more effective by shallow thermocline depth, itself strongly
 669 influenced by remote forcing. The seasonal cycle in the CLR is modulated by strong year-to-year variations, as

670 observed in boreal spring 2005 when cold SST anomaly are associated with shallower-than-average thermocline
671 depth and positive wind speed anomaly.

672 The intraseasonal wind bursts which occurred in boreal spring 2005 and 2006 generated cooling episodes
673 especially around 3°-4° S except for some strongest events when the cooling reached more northern equatorial
674 region, especially during the mid-May and end-May 2005 events. The intensity of the cold events resulted from
675 both basin preconditioning by remotely forced shoaling of the thermocline (via Kelvin wave), local mixing
676 (induced by current vertical shear) and upwelling processes in response to strong southerly local winds. For one
677 particular event, on 26-28 May 2005, the net heat flux also tended to cool the surface water, due to enhanced
678 cloud cover which decreased the incoming solar radiations. In the CLR, stronger wind intensification and
679 favorably preconditioned oceanic subsurface conditions in 2005 made the coupling between surface and
680 subsurface ocean processes more efficient than in 2006, resulting in stronger cooling. It should be noted that the
681 occurrence of intraseasonal wind intensification in the CLR is not specific to the boreal spring/summer 2005 and
682 2006 and is observed every year over the 1998-2008 period of study (not shown). However, their impact on
683 SST variability in the region is modulated depending of the strength of wind intensification and of the
684 subsurface preconditioning. For example, the year 1998, known as a "warm year", is characterized by
685 anomalous warm SST in boreal spring/summer in the CLR., associated with anomalous weak winds and
686 anomalous deep thermocline.

687 The preconditioning of subsurface conditions in the area via Kelvin wave at the dates of the wind bursts
688 depended on the atmospheric conditions in the western part of the basin a few weeks earlier. Previous studies
689 (e.g. Picaut, 1983; Philander, 1990) suggest that the source of an equatorial Kelvin wave is mainly related to a
690 sudden change of the zonal wind in the west. Analysis of atmospheric and oceanic conditions at intraseasonal to
691 daily scale in winter 2005 and 2006 showed that for both years, an Kelvin upwelling wave was initiated in the
692 west while easterly winds were strengthened from either side of the equator just after the ITCZ to be at its
693 southernmost location. This latter was observed one month earlier in 2006 (late February – early March) than in
694 2005 (late March-early April), and was associated with a negative wind stress curl anomaly. In winter 2005, the
695 ITCZ was found south of the equator after a very sudden southward shift and was followed by strong easterlies
696 during ~20 days, while in winter 2006, the ITCZ was found closer to the equator less sharply and during a
697 longer period, followed by weaker easterlies when compared to 2005. These results obtained for the years 2005
698 and 2006 years do not imply that same atmospheric conditions would be observed for winter upwelling Kelvin
699 wave of other years. Especially, the year 2005 was very particular and also exhibited anomalously cold SSTs in
700 the south Atlantic and anomalously warm SSTs in the north Atlantic initiated in fall 2004, signature of a
701 meridional mode (Virmani and Weisberg, 2006; Foltz and Mc. Phaden, 2006; Hormann and Brandt, 2009).

702 Upon impingement at the eastern boundary, the incoming equatorial Kelvin wave excites westward-propagating
703 Rossby waves and poleward propagating coastal Kelvin waves. In 2005, the Kelvin wave reached the coast
704 around mid-May while southerly winds strengthened, allowing the reflected wave to be reinforced by the local
705 wind. This resulted in westward propagation of negative z_{20} and SSH anomalies which, combined with

706 enhanced westward surface currents, provided favorable conditions to westward extension of cold upwelled
707 water from the eastern coast to near 20°W through advection and vertical mixing.

708

709

710 In the second part of the study, we specially focused on the mid-May 2005 event (13 May to 16 May) that was
711 characterized by strong southerly wind strengthening in the eastern Tropical Atlantic Ocean. It was found to be
712 responsible for the sudden and intense SST cooling in the Gulf of Guinea and the CLR, and involved in the early
713 onset of the ACT development in 2005 and therefore in early onset of the WAM. The analysis of atmospheric
714 and oceanic conditions in the Gulf of Guinea associated to this event allowed to show that the mid-May event,
715 controlled by the St. Helena Anticyclone, can be identified as a “decisive event” which triggered the abrupt
716 transition between two wind patterns in the northern Gulf of Guinea. Unusual strong southerly winds induced
717 anomalously strong equatorial cooling which in turns slowed down the overlying wind feedback mechanism and
718 generated stronger than normal southerlies north of the equator through the SST front around 1°N. This
719 triggered the deep atmospheric convection in the Gulf of Guinea at a self-sustaining level and the beginning of
720 coastal precipitation. The time of occurrence of this phenomenon, 15 days earlier than the averaged date (31
721 May from Leduc-Leballeur et al., 2013), suggests that the mid-May 2005 event was associated with anomalous
722 strong moisture flux. The description of atmospheric conditions over the 1998-2008 period has shown that the
723 2005 event was characterized by the strongest surface pressure gradient between the St. Helena high pressures
724 and the low pressures under the ITCZ, inducing strong Hadley cell activity. No similar atmospheric pattern was
725 observed during the whole 1998-2008 period. Another wind burst of comparable wind intensity occurred at the
726 beginning of May 2000. This event also induced a cooling at the equator but the surface pressure decrease in
727 ITCZ region was not as pronounced than during mid-May 2005 event and the SST gradient around 1° N was
728 weaker. In addition to coastal precipitation in the Gulf of Guinea and due to the early cooling in the ACT region,
729 unusually rainfall conditions also occurred between the northeast coast of Brazil and 15° W within the SITCZ,
730 which generally forms in early boreal summer.

731 Finally, this study highlights the impact of a strong southerly wind burst in the eastern tropical Atlantic during
732 boreal spring season, which is a transitional period during which an anomalous strong energy input may tip the
733 energy balance from an equilibrium state toward another one and thus impact the WAM system. The analysis of
734 atmospheric and oceanic conditions during the mid-May 2005 wind event allows to highlight the different
735 processes through which the wind power provided by the wind burst is brought to the ocean: i) direct effect of
736 the wind on the SST in the eastern tropical Atlantic; ii) changes in the trade winds in the western equatorial
737 Atlantic exciting eastward-propagating equatorial Kelvin waves; iii) energy transport via atmospheric gravity
738 waves from South Atlantic; and iv) energy supply to Rossby wave. In addition to unusual atmospheric
739 conditions in mid-May 2005, the ocean response intensity to this event was also enhanced by the subsurface
740 conditions, made favorable by previous wind bursts, either local (e.g. in 6-8 May) or occurring a few weeks
741 before in the West.

742 It is crucial to better describe the atmospheric and oceanic processes in play during such extreme event, notably
743 in order to reduce the well known warm bias in the southeastern tropics in coupled models in both atmospheric
744 and oceanic components (Zeng et al., 1996; Davey et al., 2002; Deser et al., 2006; Chang et al., 2007; Richter
745 and Xie, 2008) as well as in forced ocean-only simulations (e.g. Large and Danabasoglu, 2006). This warm bias
746 is well evidenced in our numerical simulation (Fig. 1&2) and our results clearly show that the cooling episodes
747 were underestimated in the CLR, implying the need to investigate more in depth the oceanic and atmospheric
748 processes in play in this particular region. As the intraseasonal wind bursts are related to the fluctuations of St.
749 Helena Anticyclone, their impact on SST variability in the eastern tropical Atlantic and regional climate
750 suggests the need of better understand the St. Helena Anticyclone variability.

751 It is also important to note that the mid-May 2005 event occurred during an unusually active year. The year
752 2005 exhibited a pronounced meridional mode pattern with strong SST gradient between the two hemispheres.
753 Several authors (Foltz et al., 2006 ; Virmani and Weisberg, 2006 ; Marengo et al., 2008a, 2008b ; Zeng et al.,
754 2008) studied this particular year, marked by anomalously warm SST in the tropical North Atlantic during
755 March-July, the warmest from at least 150 years. This anomalous warming was associated with the most active
756 and destructive hurricane season on record (Foltz et al., 2006; Virmani and Weisberg, 2006) and an extreme and
757 rare drought in the Amazon Basin (Marengo et al., 2008a, 2008b; Zeng et al. 2008; Erfanian et al., 2017). From
758 these authors, primary causes of the anomalous warming in 2005 were a weakening of the northeasterly trade
759 winds and associated decrease in wind-induced latent heat loss as well as changes in shortwave radiation and
760 horizontal oceanic heat advection. This 2005 temperature record is made even more remarkable given that,
761 unlike the 1998's one, it occurred in the absence of any strong El Niño anomaly (Shein, 2006). Some studies
762 (Goldenberg et al., 2001) attribute these SST increases to the Atlantic Multidecadal Oscillation (AMO), while
763 others suggest that climate change may instead be playing the dominant role (Emanuel, 2005; Webster et al.,
764 2005; Mann and Emanuel, 2006; Trenberth and Shea, 2006). Comparable anomalously warm tropical Atlantic
765 SSTs have been observed in 2010 also associated with extreme drought in the Amazon. However, from time
766 series of monthly anomalies constructed for the two basins (North and South Atlantic) by using OISST monthly
767 mean data, Erfanian et al. (2017) show that the warmer-than-usual SSTs in the North Atlantic in 2010 was not
768 associated with colder-than-usual SST in South Atlantic contrarily to 2005 (their Fig. S4e).

769 While the warming in North Tropical Atlantic during 2005 has been investigated by several authors, the cooling
770 in South Atlantic has received less attention. This study highlights the need to further document and monitor the
771 South Atlantic region and the St. Helena Anticyclone, through additional high resolution analysis and
772 observations.

773

774 Acknowledgments:

775 The research leading to these results received funding from the EU FP7/2007-2013 under grant agreement no.
776 603521, PREFACE and from the EU Horizon 2020 under grand agreement no. 2014-633211, AtlantOS. These

777 projects are gratefully acknowledged. We do thank Gildas Cambon for his help and participation on the
778 implementation of ROMS simulations, and Frédéric Marin for his helpful comments.

779

780 **References:**

781

782 Adamec, D., O'Brien, J. J.: The seasonal upwelling in the Gulf of Guinea due to remote forcing, *J. Phys.*

783 *Oceanogr.*, 8, 1050-1060, 1978.

784

785 Battisti, DS.: Dynamics and thermodynamics of a warming event in a coupled tropical atmosphere ocean model,

786 *J. Atmos. Sci.* 45:2889 – 2919, 1988.

787

788 Busalacchi, A., Picaut, J.: Seasonal variability from a model of the tropical Atlantic Ocean, *J. Phys Oceanogr.*,

789 13, 1564-1588, 1983.

790

791 Bourlès, B., Brandt, P., Caniaux, G., Dengler, M., Gouriou, Y., Key, E., Lumpkin, R., Marin, F., Molinari, R.L.,

792 Schmid, C. : African Monsoon Multidisciplinary Analysis (AMMA): Special measurements in the

793 Tropical Atlantic, CLIVAR Exchange Letters, 41 (12 2), International CLIVAR Project Office,

794 National Oceanography Centre, Southampton, United Kingdom, 7–9, 2007.

795

796 Brandt, P., Funk, A., Hormann, V., Dengler, M., Greatbatch, R.J., Toole, J.M.: Interannual atmospheric

797 variability forced by the deep equatorial Atlantic Ocean, *Nature*, 473, 497–500,

798 doi:10.1038/nature10013, 2011.

799

800 Caniaux, G., Giordani, H., Redelsperger, J.-L., Guichard, F., Key, E., Wade, M.: Coupling between the Atlantic

801 cold tongue and the West African monsoon in boreal spring and summer, *J. Geophys. Res.*, 116,

802 C04003, doi:10.1029/2010JC006570, 2011.

803

804 Carton, J. A., Chepurin, G., Cao, X., Giese, B.S.: A simple ocean data assimilation analysis of the global upper

805 ocean 1950 –1995, part 1: Methodology, *J. Phys. Oceanogr.*, 30, 294–309, doi:10.1175/ 1520-

806 0485(2000)030<0294:ASODAA>2.0.CO;2, 2000a.

807

808 Carton, J. A., Chepurin, G., Cao, X.: A simple ocean data assimilation analysis of the global upper ocean 1950–

809 1995, part 2: Results, *J. Phys. Oceanogr.*, 30,311–326, doi:10.1175/1520-0485(2000)

810 030<0311:ASODAA>2.0.CO;2, 2000b.

811

812 Carton, J. A., and Giese, B.S.: A reanalysis of ocean climate using simple ocean data assimilation (SODA),

813 *Mon. Weather Rev.*, 136 ,2999–3017, doi:10.1175/2007MWR1978.1, 2008.

814

815 Colin, C.: Sur la variabilité dans le Golfe de Guinée: Nouvelles considérations sur les mécanismes d'upwelling,
816 Ph.D. thesis, Mus. Natl. d'Hist. Nat., Paris, 1989.
817

818 Chang, C.-Y., Carton, J.A., Grodsky, S.A., Nigam, S.: Seasonal climate of the tropical Atlantic sector in the
819 NCAR Community Climate System Model 3: Error structure and probable causes of errors, *J. Climate*,
820 20, 1053–1070, 2007.
821

822 Chelton, D. B., deSzoeke, R.A., Schlax, M. G. , Naggar, K. E., Siwertz, N.: Geographical variability of the first-
823 baroclinic Rossby radius of deformation, *J. Phys. Oceanogr.*, 28, 433–460, 1998.
824

825 Dai, A., and Trenberth, K.E.: Estimates of freshwater discharge from continents: Latitudinal and seasonal
826 variations, *J. Hydrometeorol.*, 3, 660–687, 2002.
827

828 Danabasoglu, G., Large, W.G., Tribbia, J.J., Gent, P.R., Briegleb, B.P.: Diurnal Coupling in the Tropical
829 Oceans of CCSM3, *Journal of Climate*, 19, 2347-2365, 2006.
830

831 Davey, M., Huddleston, M., Sperber, K.R., et al.: STOIC: A study of coupled model climatology and variability
832 in tropical ocean regions, *Clim. Dynam.*, 18, 403-420, 2002.
833

834 Debreu, L., Marchesiello, P., Penven, P., Cambon, G.: Two-way nesting in split-explicit ocean models:
835 algorithms, implementation and validation, *Ocean Modelling*, 49-50, 1-21, 2012.
836

837 De Coëtlogon, G., Janicot, S., Lazar, A.: Intraseasonal variability of the ocean-atmosphere coupling in the Gulf
838 of Guinea during boreal spring and summer, *Q. J. R. Meteorol. Soc.*, 136, 426–441, doi:10.1002/qj.554,
839 2010.
840

841 Denamiel, C., Budgell, W.P., Toumi, R.: The Congo River plume: Impact of the forcing on the far-field and
842 near-field dynamics, *J. Geophys. Res. Oceans*, 118, 964–989, doi:10.1002/jgrc.20062, 2013.
843

844 Deser, C., Capotondi, A., Saravanan, R., Phillips, A.: Tropical Pacific and Atlantic climate variability in
845 CCSM3, *J. Climate*, 19, 2451–2481, 2006.
846

847 Djakouré, S., Penven, P., Bourlès, B., Veitch, J., Koné, V.: Coastally trapped eddies in the north of the Gulf of
848 Guinea, *J. Geophys. Res. Oceans*, 119, 6805–6819, doi:10.1002/2014JC010243, 2014.
849

850 Emanuel, K.: Increasing destructiveness of tropical cyclones over the past 30 years, *Nature*, 436, 686-688, 2005.
851

852 Erfanian, A., Wang, G., Fomenko, L.: Unprecedented drought over tropical South America in 2016:
853 significantly under-predicted by tropical SST, *Scientific reports*, 7:5811, doi: 10.1038/s41598-
854 017_05373-2, 2017.

855

856 Foltz, G. R., Grodsky, S. A., Carton, J. A., McPhaden, M. J.: Seasonal mixed layer heat budget of the tropical
857 Atlantic Ocean, *J. Geophys. Res.*, 108, 3146, doi:10.1029/2002JC001584, 2003.

858

859 Foltz, G.R. and McPhaden, M.J.: Unusually warm sea surface temperatures in the tropical North Atlantic during
860 2005, *Geophys. Res. Lett.*, 33: doi: 10.1029/2006GL027394. issn: 0094-8276, 2006.

861

862 Fritts, D. C.: Wave saturation in the middle atmosphere: A review of theory and observations, *Rev. Geophys.*,
863 22, 275–308, 1984.

864

865 Gentemann, C.L., Wentz, F.J., Brewer, M., et al.: Passive Microwave Remote Sensing of the Ocean: an
866 Overview, *Oceanography from Space, Revisited*, edited by V. Barale, J. Gower, and L. Alberotanza,
867 13–33. Heidelberg: Springer, 2010.

868

869 Giese, B.J, Harrison, D.E.: Aspects of the Kelvin wave response to episodic wind forcing, *J. Geophys. Res.*, 95:
870 7289 – 7312, 1990.

871

872 Giordani, H., Caniaux, G., Voldoire, A.: Intraseasonal mixed-layer heat budget in the equatorial Atlantic during
873 the cold tongue development in 2006, *J. Geophys. Res.: Oceans*, 118(2):650-671. doi:
874 10.1029/2012JC008280, 2013.

875

876 Goldenberg, S.B., Landsea, C.W., Mestas-Nuñez, A.M., Gray, W.M.: The Recent Increase in Atlantic Hurricane
877 Activity: Causes and Implications, *Sciences*, Vol. 293, Issue 5529, pp. 474-479, doi:
878 10.1126/science.1060040, 2001.

879

880 Grodsky, S. A., Carton, J. A.: The Intertropical Convergence Zone in the South Atlantic and the Equatorial Cold
881 Tongue, *J. Climate*, 16, 723–733, 2003.

882

883 Haidvogel, D.B., Beckmann, A.: *Numerical Ocean Circulation Modeling*, Imperial College Press, London; 320
884 pp., 1999.

885

886 Herbert, G., Bourlès, B., Penven, P., Grelet, J.: New insights on the upper layer circulation north of the Gulf of
887 Guinea, *J. Geophys. Res.: Oceans*, 121, doi:10.1002/2016JC011959, 2016.

888

889 Hormann, V., Brandt, P.: Upper equatorial Atlantic variability during 2002 and 2005 associated with equatorial
890 Kelvin waves, *J. Geophys. Res.*, 114: C03007, doi:10.1029/2008JC005101, 2009.
891

892 Illig, S., Dewitte, B., Ayoub, N., du Penhoat, Y., Reverdin, G., Mey, P.D., Bonjean, F., Lagerloef, G.S.E.:
893 Interannual long equatorial waves in the tropical Atlantic from a high-resolution ocean general
894 circulation model experiment in 1981-2000, *J. Geophys. Res.: Oceans*, 109:C02022. doi: 10.1029/
895 2003JC001771, 2004.
896

897 Jouanno, J., Marin, F., duPenhoat, Y., Sheinbaum, J., Molines, J.M.: Seasonal heat balance in the upper 100m of
898 the Equatorial Atlantic Ocean, *J. Geophys. Res.: Oceans*, 116:C09003. doi: 10.1029/2010JC006912,
899 2011.
900

901 Jouanno, J., Marin, F., duPenhoat, Y., Molines, J.M.: Intraseasonal Modulation of the Surface Cooling in the
902 Gulf of Guinea, *J. Phys. Oceanogr.*, 43(2):382-401. doi: 10.1175/JPO-D-12-053.1, 2013.
903

904 Krishnamurti, T. N., Pasch, R.J., Ardanuy, P.: Prediction of African waves and specification of squall lines,
905 *Tellus*, 32, 215-231, 1980.
906

907 Leduc-Leballeur, M., Eymard, L., de Coëtlogon, G.: Observation of the marine atmospheric boundary layer in
908 the Gulf of Guinea during the 2006 boreal spring, *Q. J. R. Meteorol. Soc.*, 137: 992 – 1003, 2011.

909 Leduc-Leballeur, M., de Coëtlogon, G., Eymard, L.: Air – sea interaction in the Gulf of Guinea at intraseasonal
910 time-scales: Wind bursts and coastal precipitation in boreal spring, *Q. J. R. Meteorol. Soc.*, 139, 387–
911 400, doi:10.1002/qj.1981, 2013.
912

913 Lübbecke, J.F., Burls, N.J., Reason, C.J.C., McPhaden, M.J.: Variability in the South Atlantic Anticyclone and
914 the Atlantic Nino Mode, *J. Climate*, 27, doi: 10.1175/JCLI-D-14-00202.1, 2014.
915

916 Mann, M. E., and Emanuel, K.A.: Atlantic hurricane trends linked to climate change, *Eos, Trans. Amer.*
917 *Geophys. Union*, 87, 233–244, 2006.
918

919 Marengo, J. A., Nobre, C.A., Tomasella, J., Oyama, M.D., De Oliveira, G.S., De Oliveira, R., Camargo, H.,
920 Alves, L.M., Brown, I.F. : The drought of Amazonia in 2005, *J. Climate*, 21, 495-516, 2008a.
921

922 Marengo, J.A., Nobre, C.A., Tomasella, J., Cardoso, M.F., Oyama, M.D.: Hydro-climatic and ecological
923 behaviour of the drought of amazonia in 2005, *Philosophical transactions of the Royal society of*
924 *London, Biological sciences*, v.21, p.1-6, 2008b.
925

926 Marin, F., Caniaux, G., Bourlès, B., Giordani, H., Gouriou, Y., Key, E.: Why were sea surface temperatures so
927 different in the Eastern Equatorial Atlantic in June 2005 and 2006, *J. Phys. Oceanogr.*, 39, 1416–1431,
928 doi:10.1175/2008JPO4030.1, 2009.

929

930 Materia, S., Gualdi, S., Navarra, A., Terray, L.: The effect of Congo River freshwater discharge on Eastern
931 Equatorial Atlantic climate variability, *Clim. Dynam.*, 39(9-10), 2109–2125, doi:10.1007/s00382-012-
932 1514-x, 2012.

933

934 McCreary, J.: Eastern tropical ocean response to changing wind systems with application to El Nino, *J. Phys.*
935 *Oceanogr.*, 6, 632-645, 1976.

936

937 McCreary, J., Picaut, J., Moore, D.: Effects of the remote annual forcing in the eastern tropical Atlantic Ocean,
938 *J. Mar. Res.*, 42, 45–81, 1984.

939

940 Merle, J. : Conditions hydrologiques saisonnières de la marge continentale du Gabon et du Congo (de 10°N a
941 60°S) Etude descriptive, *Dot. Sci. O.R.S.T.O.M. Pointe-Noire*, 27 : 1-20, 1972.

942

943 Merle, J., Fieux, M., Hisard, P.: Annual signal and interannual anomalies of sea surface temperature in the
944 eastern equatorial Atlantic Ocean, *Deep Sea Res.*, 26,77–101, 1980.

945

946 Mitchell, T. P., Wallace, J.M.: The annual cycle in equatorial convection and sea surface temperature, *J.*
947 *Climate*, 5, 1140–1156, 1992.

948

949 Moore, D.W.: Planetary-gravity waves in an equatorial ocean, PhD Thesis, Harvard University, 201 pp., 1968.

950

951 Moore, D.W., and Philander, S.G.H.: Modeling of the tropical ocean circulation, *The Sea*, Vol. 6, Wiley
952 Interscience, New York, N.Y., pp. 316-361, 1977.

953

954 Moore, D. W., Hisard, P., McCreary, J. P., Merle, J., O'Brien, J. J., Picaut, J., Verstraete, J. M., Wunsch, C.:
955 Equatorial adjustment in the eastern Atlantic, *Geophys. Res. Lett.*, 5, 637-640, 1978.

956

957 Nguyen, H., Thorncroft, C. D., Zhang, C.: Guinean coastal rainfall of the West African Monsoon, *Q.J.R.*
958 *Meteorol. Soc.*, 137: 1828–1840. doi:10.1002/qj.867, 2011.

959 Nicholson, S.E., Dezfuli, A.K.: The relationship of rainfall variability in western equatorial Africa to the tropical
960 oceans and atmospheric circulation. Part I: The boreal spring, *J. Climate*, 26(1), 45–65, 2013.

961 Nobre, P., Shukla, J.: Variations of sea surface temperature, wind stress, and rainfall over the tropical Atlantic
962 and South America, *J. Climate*, 9 : 2464 – 2479, 1996.

963

964 Okumura, Y., and Xie, S.P.: Interaction of the Atlantic equatorial cold tongue and the African monsoon, *J.*

965 *Climate*, 17, 3589–3602, 2004.

966

967 Okumura, Y., Xie, S.P.: Some overlooked features of tropical Atlantic climate leading to a new Niño-like

968 phenomenon, *J. Climate*, 19(22), 5859–5874, doi:10.1175/JCLI3928.1, 2006.

969

970 Penven, P., Marchesiello, P., Debreu, L., Lefevre, J.: Software tools for pre- and post-processing of oceanic

971 regional simulations, *Environ. Modell. Software*, 23, 2008 660–662, 2008.

972

973 Peter, A.-C., Le Hénaff, M., du Penhoat, Y., Menkès, C., Marin, F., Vialard, J., Caniaux, G., Lazar, A.: A model

974 study of the seasonal mixed layer heat budget in the equatorial Atlantic, *J. Geophys. Res.*, 111, C06014,

975 doi: 10.1029/2005JC003157, 2006.

976

977 Philander, S., and Pacanowski, R.: A model of the seasonal cycle in the Tropical Atlantic Ocean, *J. Geophys.*

978 *Res.*, 91, 14, 192–14, 206, 1986.

979

980 Philander, S.G.: *El Nino, La Nina and the Southern Oscillation*, Academic Press, 293 pp., 1990.

981

982 Picaut, J.: Propagation of the seasonal upwelling in the eastern equatorial Atlantic, *J. Phys. Oceanogr.*, 13, 18–

983 37, doi: 10.1175/1520-0485, 1983.

984

985 Picaut, J.: On the dynamics of the thermal variations in the Gulf of Guinea, *Oceanogr. Trop.*, 19 (2) : 127-53,

986 1984.

987

988 Piton, B. : Les courants sur le plateau continental devant Pointe-Noire (Congo), *Documents scientifiques*,

989 ORSTOM, Brest, n°47, 37 p., 1988.

990

990 Polo, I., Lazar, A., Rodriguez-Fonseca, B., Arnault, S.: Oceanic Kelvin waves and tropical Atlantic

991 intraseasonal variability: 1. Kelvin wave characterization, *J. Geophys. Res.*, 113, C07009, doi: 10.1029/

992 2007JC004495, 2008.

993

994 Redelsperger, J. L., et al. : AMMA: Une étude multidisciplinaire de la mousson Ouest-Africaine, *Meteorologie*,

995 54,22–32, doi:10.4267/2042/20098, 2006.

996

997 Richter, I. and Xie, S.-P.: On the origin of equatorial Atlantic biases in coupled general circulation models,

998 *Clim. Dynam.*, 1:587–598, doi : 10.1007/s00382-008-0364-z, 2008.

999 Rouault, M., Servain, J., Reason, C. J. R. , Bourlès, B., Rouault, M. J. , Fauchereau, N.: Extension of PIRATA
1000 in the tropical south-east Atlantic: An initial one-year experiment, *Afr. J. Mar. Sci.*,31(1),63–71,
1001 doi:10.2989/AJMS.2009.31.1.5.776, 2009.

1002

1003 Saha, S., Moorthi, S., Pan, H.-L., Wu, W., Wang, J., Nadiga, S., Tripp, P., Kistler, R., Woollen, J., Behringer,
1004 D., Liu, H., Stokes, D., Grumbine, R., Gayno, G., Wang, J., Hou, Y.T., Chuang, H.-Y., Juang, H.-M.
1005 H., Sela, J., Iredell, M., Treadon, R., Kleist, D., Van Delst, P., Keyser, D., Derber, J., Ek, M., Meng, J.,
1006 Wei, H., Yang, R., Lord, S., Van Den Dool, H., Kumar, A., Wang, W., Long, C., Chelliah, M., Xue, Y.,
1007 Huang, B., Schemm, J.-K., Ebisuzaki, W., Lin, R., Xie, P., Chen, M., Zhou, S., Higgins, W., Zou, C.-Z.
1008 Z., Liu, Q., Chen, Y., Han, Y., Cucurull, L., Reynolds, R.W., Rutledge, G., Goldberg, M. : The NCEP
1009 climate forecast system reanalysis, *Amer. Meteor. Soc.*, 91, 1015-1057, 2010.

1010

1011 Schouten, M. W., Matano, R. P., Strub, T. P.: A description of the seasonal cycle of the equatorial Atlantic from
1012 altimeter data, *Deep Sea Res., Part I*, 52, 477–493, doi:10.1016/j.dsr.2004.10.007, 2005.

1013

1014 Servain, J., Picaut, J., Merle, J.: Evidence of remote forcing in the equatorial Atlantic Ocean, *J. Phys. Oceanogr.*,
1015 12, 457–463, 1982.

1016

1017 Shein, K. A.: State of the climate in 2005, *Bull. Am. Meteorol. Soc.*, 87, s1–s102, doi: 10.1175/BAMS-87-6-
1018 shein, 2006.

1019

1020 Shchepetkin, A., McWilliams, J.C.: The Regional Oceanic Modeling System (ROMS): A split-explicit, free-
1021 surface, topography-following-coordinate ocean model, *Ocean Modell.* 9, 347–404, 2005.

1022

1023 Thorncroft, C. D., Nguyen, H., Zhang, C., Peyrillé, P.: Annual cycle of the West African monsoon: regional
1024 circulations and associated water vapour transport, *Q. J. R. Meteorol. Soc.*, 137, 129-147,
1025 doi:10.1002/qj.728, 2011.

1026

1027 Trenberth, K.E., Shea, D.J.: Atlantic hurricanes and natural variability in 2005, *Geophys. Res. Lett.*, vol. 33,
1028 L12704, doi: 10.1029/2006GL026894, 2006.

1029

1030 Virmani, J. I., and Weisberg, R.H.: The 2005 hurricane season: An echo of the past or a harbinger of the future?,
1031 *Geophys. Res. Lett.*, 33, L05707, doi: 10.1029/2005GL025517, 2006.

1032

1033 Wade, M., Caniaux, G., du Penhoat, Y.: Variability of the mixed layer heat budget in the eastern equatorial
1034 Atlantic during 2005–2007 as inferred using Argo floats, *J. Geophys. Res.*, 116, C08006, doi:
1035 10.1029/2010JC006683, 2011.

1036

1037 Yu, L., Jin, X., Weller, R.A.: Role of net surface heat flux in seasonal variations of sea surface temperature in
1038 the tropical Atlantic ocean, *J. Climate*, 19, 6153–6169, 2006.
1039
1040 Waliser, D. E., and Gautier, C.: A satellite-derived climatology of the ITCZ, *J. Climate*, 6, 2162–2174, 1993.
1041
1042 Wauthy, B. : Introduction à la climatologie du Golfe de Guinée, *Oceanogr. Trop.*, 18, 103–138, 1983.
1043
1044 Webster, P.J., Holland, G. J., Curry, A., Chang, H.R.: Changes in tropical cyclone number, duration, and
1045 intensity, in warming environment, *Science*, 309, 1844-1846, 2005.
1046
1047 Wentz, F.J., and Meissner, T.: Algorithm Theoretical Basis Document (ATBD), version 2, AMSR-E Ocean
1048 Algorithm, Remote Sensing Systems Tech. Rep., RSS 121599A-1, 55 pp., 2000.
1049
1050 White, R.H. and Toumi, R.: River Flow and Ocean Temperatures: The Congo River, *J. Geophys. Res. -Oceans*,
1051 119, 25016–2517, doi:10.1002/2014JC009836, 2014.
1052
1053 Zebiak, S.: Air-sea interaction in the equatorial Atlantic region, *J. Climate*, 6(8), 1567–1586, doi:10.1175/1520-
1054 0442(1993)006<1567:AIITEA>2.0.CO;2, 1993.
1055
1056 Zeng, N., Dickinson, R.E., Zeng, X.: Climatic impact of Amazon deforestation-A mechanistic model study, *J.*
1057 *Climate*, 9, 859–883, 1996.
1058
1059 Zeng, N., Dickinson, R.E., Zeng, X.: Causes and impacts of the 2005 Amazon drought, *Env. Res. Lett.*, 3, doi:
1060 10.1088/1748-9326/3/1/014002, 2008.